



Incorporating adult age into mosquito population models: Implications for predicting abundances in changing climates

Renato Andrade ^{a,*}, Steven M. White ^c, Christina A. Cobbold ^{a,b}

^a School of Mathematics and Statistics, University of Glasgow, Glasgow G12 8QQ, UK

^c UK Centre for Ecology & Hydrology, Benson Lane, Wallingford, Oxfordshire OX10 8BB, UK

^b Boyd Orr Centre for Population and Ecosystem Health, University of Glasgow, Glasgow G12 8QW, UK

ARTICLE INFO

Keywords:

Mosquito population dynamics
Senescence
Climate change
Culex pipiens
Seasonality
Stage-structured model

ABSTRACT

Mosquito-borne diseases (MBDs) pose increasing threats under future climate change scenarios and an understanding of mosquito population dynamics is pivotal to predicting future risk of MBDs. Most models that describe mosquito population dynamics often assume that adult life-history is independent of adult age and yet mosquito senescence is known to affect mosquito mortality, fecundity and other key biological traits. Despite this, little is known about the effects of adult age at the level of the mosquito population, especially under varying temperature scenarios. We develop a stage-structured delayed differential equations (DDEs) model incorporating the effects of the abiotic environment and adult age to shed light on the complex interactions between age, temperature, and mosquito population dynamics. Taking *Culex pipiens*, a major vector of West Nile Virus, as our study species our results show that failing to consider mosquito senescence can lead to underestimates of future mosquito abundances predicted under climate change scenarios. We also find that the age-dependent mechanisms combined with the effects of density-dependent mortality on the immature stages can result in mosquito abundances decreasing at extreme temperatures. With our work, we underscore the need for more studies to consider the effects of mosquito age. Not accounting for senescence can compromise the accuracy of abundance estimates and has implications for predicting the risk of future MBD outbreaks.

1. Introduction

Vector-borne diseases (VBDs) such as dengue, malaria, and leishmaniasis impose significant health and economic burdens on human populations, causing millions of deaths annually and leading to high economic costs due to hospitalizations and lost productivity from illness (World Health Organization et al., 2020). In the recent decades, VBDs have re-emerged in locations in which they were once eradicated and spread to territories in which they were previously absent (Chala and Hamde, 2021; El-Sayed and Kamel, 2020). The causes for the emergence and re-emergence of VBDs include changes to vector distributions through direct human activity such as deforestation, irrigation, urbanisation (Gratz, 1999; Gangoso et al., 2020), and the impacts of climate change (Rogers and Randolph, 2006; Caminade et al., 2019; Wilson et al., 2020). Among the VBDs, the ones that pose the largest threat to present and future human health and economy are transmitted by mosquitoes (Organization, 2022; Franklins et al., 2019; Manguin and Boëte, 2011). Hence, comprehensive studies of mosquito dynamics and their role as disease vectors are vital in the bid to not only

prevent deaths but also to mitigate the economic costs on healthcare systems.

Multiple biotic and abiotic drivers shape mosquito dynamics (Hardy et al., 1983). Environmental factors such as humidity and temperature play pivotal roles in shaping mosquito life cycles and behaviour, which in turn affect mosquito-borne diseases (MBDs) risks (Mordecai et al., 2019). Given the ectothermic nature of mosquitoes, temperature strongly influences mortality rates, developmental processes, and overall activity levels (Shelton et al., 1973; Watts et al., 1987; Delatte et al., 2009). These physiological and life-history traits are often influenced by mosquito senescence in many mosquito species of human interest, such as those from the genera *Aedes*, *Anopheles* and *Culex*, due to their role in disease transmission (Turell, 2012; Brugman et al., 2018). Studies have shown for species in these genera that as mosquitoes age, their mortality rates can increase (Knecht et al., 2018; Clements and Paterson, 1981), their fecundity can decline (McCann et al., 2009; Akoh et al., 1992), and their ability to transmit diseases is affected in complex ways (Richards et al., 2009; Pigeault et al., 2015; Knecht et al., 2018; Mayton et al., 2020). Previous researches have highlighted the importance

* Corresponding author.

E-mail address: reand705@gmail.com (R. Andrade).

<https://doi.org/10.1016/j.jtbi.2025.112084>

Received 26 September 2024; Received in revised form 1 February 2025; Accepted 25 February 2025

Available online 1 March 2025

0022-5193/© 2025 The Author(s). Published by Elsevier Ltd. This is an open access article under the CC BY license (<http://creativecommons.org/licenses/by/4.0/>).

of mosquito senescence in disease transmission and in designing control strategies, as adults of different ages contribute differently to both overall population abundance and disease transmission (Styer et al., 2007a; Somé et al., 2024; Harrington et al., 2014). However, few studies have explored in detail the effects of mosquito senescence on seasonal abundance patterns, particularly in the context of future climate change scenarios, which is crucial for understanding MBD dynamics and transmission to humans.

The complex interaction of environment and ageing on individual mosquitoes present challenges when predicting the effects of age at the population level. For example, increased temperatures may reduce the duration of the immature stages and the length of the gonotrophic cycle, providing more opportunities for egg-laying (Loetti et al., 2011; Madder et al., 1983). However, as adults age, after each cycle, females tend to lay fewer eggs (Roubaud, 1944; Awahmukalah and Brooks, 1985), and face increased mortality due to senescence (Clements and Paterson, 1981). Consequently, predicting how adult abundance responds to increasing temperatures, particularly when considering the effects of senescence, remains unclear. Mathematical models provide a valuable framework for incorporating the mechanisms affecting species life-history, offering novel opportunities for insights into the dynamics of mosquito populations.

Previous studies have developed models that indicated the role ageing can play in VBDs dynamics, without explicitly accounting for the effects of temperature. By comparing an age-dependent to an age-independent model for vectorial capacity, Bellan (2010) indicated how VBD models that fail to consider age-dependent mortality can overestimate the efficiency of mosquito control strategies. They observed that the majority of the transmission happens through younger mosquitoes that survive long enough to be infected and transmit the pathogen. Similar conclusions were obtained by Rock et al. (2015), who utilised partial differential equations (PDEs) to build a VBD model that incorporated the effects of age on mosquito mortality and biting rates.

In parallel to the models that have focused on age only effects, mathematical models that concentrate on incorporating the influence of temperature on mosquito dynamics while omitting the effect of aging have shown how mosquito abundances are likely to increase in future climate scenarios. Ewing et al. (2016) proposed a detailed description of temperature mechanisms acting on mosquito biology through a delayed-differential equations (DDEs) model, later refined in Ewing et al. (2019). Despite the good fit of the Ewing et al. (2019) model to *Cx. pipiens* abundance data, the authors highlighted how the incorporation of adult senescence mechanisms could potentially further enhance the predictions of the model.

While studies have successfully explored the dynamics of mosquito populations by incorporating age and temperature mechanisms separately (Cailly et al., 2012; Metelmann et al., 2019; Bakran-Lebl et al., 2023; Frantz et al., 2024; Brass et al., 2024), there has been a limited number of models considering the temperature and age mechanisms simultaneously. One notable exception is the age-structured, discrete-time matrix mosquito population model introduced by Lončarić and Hackenberger (2013). In this model, stage duration is influenced by temperature, while adult age affects fecundity but not mortality. Lončarić and Hackenberger (2013) explore the sensitivity of transient mosquito dynamics to the different developmental stages, identifying larval and adult stages as those most sensitive and most suitable targets for control measures.

We focus on modelling a particular mosquito species, *Culex pipiens*. The seasonal abundance patterns of *Cx. pipiens* remain not fully understood. In particular, distinct explanations have been proposed for the observation that this species can often exhibit two separate population peaks per year (Barker et al., 2010; Ewing et al., 2019). Furthermore, climate change has caused noticeable range expansions for *Culex* mosquitoes (Liu et al., 2020; Hongoh et al., 2012), highlighting the notable response of these mosquito species to changing environmental con-

ditions. Notably, there has been a growing concern about the increased risk of Rift Valley Fever (RVF) transmission by *Cx. pipiens* in countries neighboring the south and east of Europe, including parts of North Africa and the Middle East (Nielsen et al., 2020). Besides RVF, other diseases, including but not limited to West Nile Virus (WNV) (Diaz-Badillo et al., 2011), Saint Louis encephalitis virus (Richards et al., 2009) and lymphatic filariasis (Ramzy et al., 2019), also feature in the repertoire of diseases transmitted by this species complex (Vinogradova, 2000). Thus understanding the seasonal abundance patterns of *Cx. pipiens* vectors is pivotal under the increasing interest on the MBDs that this species can transmit, especially in a changing climate.

We investigate the impact of climate change induced temperature increases on *Cx. pipiens* populations while examining the role of adult age dynamics. In particular, we consider the implications on the mosquito population dynamics of various hypothetical temperature scenarios based on both historic temperature recordings and future climate predictions. We build upon the previous *Cx. pipiens* model established by (Ewing et al., 2019). Our approach distinguishes itself from previous models by incorporating explicitly the effects of age on mortality and fecundity in addition to the detailed temperature dependency introduced by Ewing et al. (2016). While our modelling is focused on *Cx. pipiens*, many of our insights are likely to apply to other mosquito species that exhibit similar responses to adult senescence.

2. Model

In our study, we focused on the effects of temperature and age on adult mosquito abundance, while not addressing hydrological factors like humidity and rainfall variability. Humidity has been receiving increasingly more attention due to its effect on mosquito survival and egg production, but requires further research for integration into mechanistic models (Brown et al., 2023). Additionally, our model assumes a fixed habitat size, due to lack of data on the relationship between habitat size and precipitation variability (Shaman et al., 2010). We introduce adult senescence into the model of *Cx. pipiens* proposed by Ewing et al. (2019), based on the framework of Nisbet and Gurney (1983). As Ewing et al. (2019), we are focused on describing the subspecies *Culex pipiens pipiens* (Vinogradova, 2000) in temperate climates. The framework from Ewing et al. (2019) tracks the progression of the population through the four main developmental stages: eggs, larvae, pupae, and adults. Each of these developmental stages is temperature-dependent and is parameterised using experimental data. Their model is a stage-structured system of DDEs, in which the time t is measured in days. We keep the same structure for the immature stages (eggs, larvae, pupae) as Ewing et al. (2019). We let $E(t)$, $L(t)$, $P(t)$ denote the abundance of the immature stages: eggs, larvae and pupae, respectively, at time t . Our model modifies the adult stage to also keep track of adult age and capture the effects of senescence by including the following mechanisms:

- Adults exhibit decreased fecundity with age (Roubaud, 1944; Awahmukalah and Brooks, 1985; Walter and Hacker, 1974),
- Adults exhibit increased mortality with age (Kershaw et al., 1954; Papadopoulos et al., 2016; Makiya and Sakurai, 1975),
- The majority of adults surviving overwinter have not had their first blood meal and are mostly nulliparous (have not laid eggs) (Makiya and Sakurai, 1975; Jaenson, 1987).

To include these features we keep track of the number of gonotrophic cycles that cohorts of adults have been through. Gonotrophic cycles are only experienced by female adults, and male adults typically do not diapause and do not survive the winter (Mitchell and Briegel, 1989; Nelms et al., 2013; Farajollahi, 2005). Therefore, we make the simplifying assumption of a 1:1 sex ratio and that male adults only contribute to the dynamics through reproduction with females. We choose to model adult

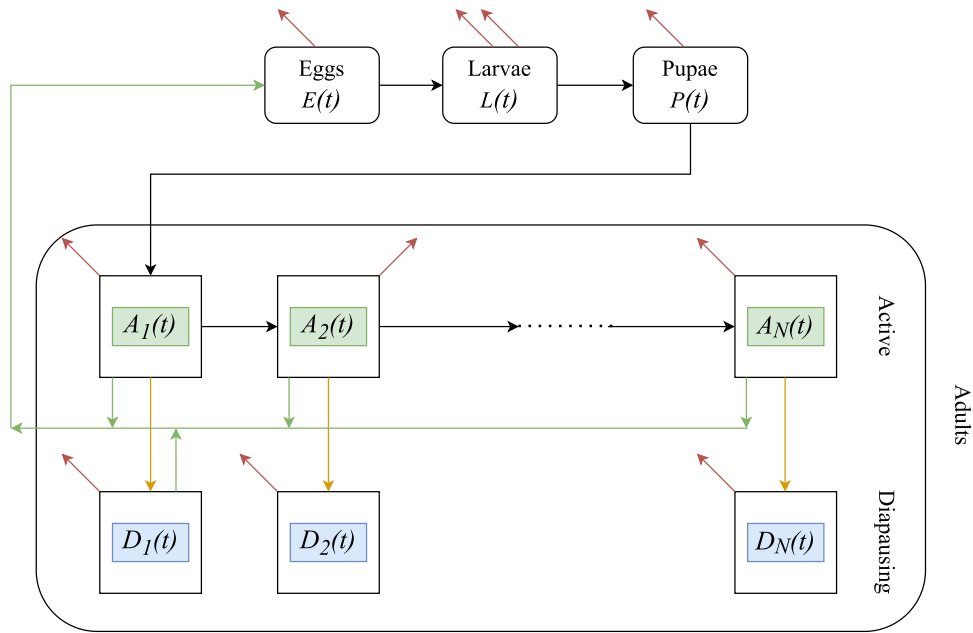


Fig. 1. Model schematic, where $E(t)$, $L(t)$, $P(t)$ correspond to the eggs, larvae and pupae sub-populations, respectively. Adult age classes are denoted by $A_j(t)$ and $D_j(t)$. After pupation is complete, individuals emerge as adults into the $A_1(t)$ class. The $D_j(t)$ classes correspond to adults that are diapausing in autumn and winter. We assume that only the $D_1(t)$ survive overwinter and therefore lay eggs after emerging from diapause in spring, dying immediately after oviposition. We refer to $A_j(t)$ as active adults and to $D_j(t)$ as diapausing adults. Black arrows: maturation of immature stages, ageing for adults. Single red arrows: density-independent mortality. Double red arrows on the larval class indicates the additional presence of density-dependent mortality. Orange arrows: diapause. Green arrows: egg-laying. Mortality, maturation and length of the gonotrophic cycle are temperature-dependent. The $D_2(t), \dots, D_N(t)$ adults are assumed not to survive the winter and hence do not lay eggs.

age by the number of gonotrophic cycles completed for two reasons. The first is that quantifying adult age from the reproductive history is a standard empirical technique (Tyndale-Biscoe, 1984; Samarawickrema, 1967) and has been successfully used to keep track age in other models (Davis et al., 2024; Kamgang et al., 2014). Secondly, experiments have tracked the increasing mortality (Clements and Paterson, 1981) and decreasing fecundity (Roubaud, 1944; Awahmukalah and Brooks, 1985) of adult mosquitoes across gonotrophic cycles, albeit not controlling for temperature. The underlying assumption is that the number of gonotrophic cycles is representative of the chronological age of mosquitoes, which is reasonable when female adults are not resource-limited (i.e., easy access to blood meals, energy and water reservoirs Vinogradova, 2000).

The model structure is illustrated in Fig. 1. The adult class is divided into N classes, $A_j(t)$, $j \in \{1, \dots, N\}$ where each $A_j(t)$ represents a different age class. After pupation is complete, individuals emerge as adults into the adult class 1, $A_1(t)$. Ageing is then represented by individuals advancing from class $A_j(t)$ to $A_{j+1}(t)$. Each $A_j(t)$ class has a different fecundity and mortality rate. We assume that the development time from class j to $j + 1$ (i.e., the length of the gonotrophic cycle) is determined by temperature and it is denoted by the variable $\tau_G(t)$. We also introduce N additional adult classes, $D_j(t)$, $j \in \{1, \dots, N\}$ to which adults transition at the onset of diapause (individuals in $A_1(t)$ transition to $D_1(t)$, $A_2(t)$ to $D_2(t)$, etc.). The $D_j(t)$ class corresponds to adults that are in diapause during autumn and winter and that only lay eggs after the overwintering period, dying immediately after egg-laying, as modelled by Ewing et al. (2019). We refer to $A_j(t)$ as active adults and to $D_j(t)$ as diapausing adults. The $D_j(t)$ individuals do not advance through the gonotrophic cycles. In Section 3.1, we show that allowing all diapausing classes to survive winter leads to a poorer fit to abundance data. Therefore, for the remainder of the analysis we assume that only $D_1(t)$ adults survive overwinter and contribute to the egg-laying in spring, since empirical data indicates the majority of mosquitoes that survive the overwintering period are nulliparous (Jaenson, 1987; Makiya and Sakurai, 1975; Vinogradova, 2000).

2.1. Stage-structured equations

In this section we present the equations for the stage-structured DDE population model following the framework from Nisbet and Gurney (1983). The equations describing the time evolution of each stage are given by

$$\begin{aligned} \frac{dE(t)}{dt} &= \overbrace{R_E(t)}^{\text{recruitment}} - \overbrace{M_E(t)}^{\text{maturation}} - \overbrace{\delta_E(t)E(t)}^{\text{mortality}}, \\ \frac{dL(t)}{dt} &= R_L(t) - M_L(t) - (\delta_{DD}(L(t), t) + \delta_L(t))L(t), \\ \frac{dP(t)}{dt} &= R_P(t) - M_P(t) - \delta_P(t)P(t), \\ \frac{dA_j(t)}{dt} &= R_{A_j}(t) - \delta_{A_j}(t)A_j(t) - M_{A_j}(t) - \overbrace{\eta(t)A_j(t)}^{\text{diapause}}, \quad j \in \{1, \dots, N-1\}, \\ \frac{dA_N(t)}{dt} &= R_{A_N}(t) - \delta_{A_N}(t)A_N(t) - \eta(t)A_N(t), \\ \frac{dD_j(t)}{dt} &= \eta(t)A_j(t) - \delta_{D_j}(t)D_j(t), \quad j \in \{1, \dots, N\}, \end{aligned} \tag{1}$$

where $R_i(t)$, $M_i(t)$, $\delta_i(t)$, $i \in \{E, L, P\}$, represent the immature recruitment, maturation, and density-independent mortality, respectively. Additionally, the larvae undergo density dependent mortality at rate $\delta_{DD}(L(t), t)$ as a consequence of competition for resources. The expressions for the immature recruitment, maturation, development and mortality rates follow directly from Ewing et al. (2019) and are given in Appendices A.1 and A.2.

The adult recruitment $R_{A_j}(t)$ and maturation $M_{A_j}(t)$ rates are given by

$$M_{A_j}(t) = R_{A_{j+1}}(t) = R_{A_j}(t - \tau_G(t))S_{A_j}(t) \frac{g_G(t)}{g_G(t - \tau_G(t))}, \quad j \in \{1, \dots, N-1\}, \tag{2}$$

where $S_{A_j}(t)$ is the survival of the active adult classes $A_j(t)$, $j \in \{1, \dots, N-1\}$, and $g_G(t)$ is the rate of progression through the gonotrophic cycle and determines the rate of progression through the adult age classes. The expression for $g_G(t)$ is parameterised by Ewing et al. (2019) and is given in Appendix A.2. The function $\tau_G(t)$ describes the duration of the gonotrophic cycle, and its evolution is given by

$$\frac{d\tau_G(t)}{dt} = 1 - \frac{g_G(t)}{g_G(t - \tau_G(t))}. \quad (3)$$

We choose the number of adult age classes to be $N = 10$. This is large enough so that a negligible (< 0.01) number of adults reach age class N during the egg-laying season.

Individuals leave the $A_j(t)$ class through age and temperature dependent mortality ($\delta_{A_j}(t)$) and entry into diapause ($\eta(t)$). Consequently, the survival of the active adult classes $A_j(t)$, $j \in \{1, \dots, N-1\}$, is given by

$$\begin{aligned} \frac{dS_{A_j}(t)}{dt} &= S_{A_j}(t) \left[\left(\delta_{A_j}(t - \tau_G(t)) + \eta(t - \tau_G(t)) \right) \frac{g_G(t)}{g_G(t - \tau_G(t))} - \delta_{A_j}(t) - \eta(t) \right]. \end{aligned} \quad (4)$$

For completeness, the survival of $A_N(t)$ is similar to Eq. (4) but without the $g_G(t)$ term, since $A_N(t)$ individuals are not maturing to another class by assumption.

The rate, $\eta(t)$, at which adults enter diapause is constrained to be zero when photoperiod is increasing and non-zero otherwise. Between $t = 0$ (corresponding to January 1st) and the summer solstice ($t = 172.5$ (Forsythe et al., 1995), using the northern hemisphere as a reference), photoperiod increases. Diapause is mainly characterised by the halt of ovarian development in females (Vinogradova, 2000). We use the termination of egg-laying in the data from Madder et al. (1983) as an indicator of the onset of diapause. We assume that when photoperiod is decreasing, the rate of entering diapause increases as the fraction of egg-laying adults decreases. The fraction of adults egg-laying in autumn is given by $\zeta_{\text{aut}}(t)$ and is estimated from trap data in which adults were captured when looking for a blood meal for ovarian development. The expression for $\zeta_{\text{aut}}(t)$ is given by

$$\zeta_{\text{aut}}(t) = \frac{1}{1 + \exp(\omega_{\text{aut}}(\xi_{\text{aut}} - \psi(t)))}. \quad (5)$$

The constants ξ_{aut} and ω_{aut} are parameterised by Ewing et al. (2019) and $\psi(t)$ is the photoperiod on day t , described by the model from Forsythe et al. (1995). We let Ψ denote the maximum rate that mosquitoes enter diapause, hence in autumn the rate of diapause entry is $\eta(t) = \Psi(1 - \zeta_{\text{aut}}(t))$. To estimate Ψ , we use high resolution (daily) egg-laying data from Madder et al. (1983) in the late summer/early autumn. The estimation of Ψ is detailed in Appendix A.4. The full expression for $\eta(t)$ is given by

$$\eta(t) = \begin{cases} 0, & \text{if } \text{mod}(t, 365) < 172.5, \\ \Psi(1 - \zeta_{\text{aut}}(t)), & \text{otherwise.} \end{cases} \quad (6)$$

2.2. Adult death rate

The adult mortality in the Ewing et al. (2019) model is temperature-dependent, but does not consider the effects of age. Fig. A.10 from Appendix A.5 illustrates that assuming that adult mortality does not change with age can underestimate mortality of older adults and overestimate mortality of younger adults (Papadopoulos et al., 2016; Makiya and Sakurai, 1975; Walter and Hacker, 1974; Clements and Paterson, 1981). We incorporate the effect of adult age on mortality by introducing a factor h_j multiplying the mortality rate of each adult class. We assume that, other than the effect of temperature ($T(t)$) on the length of the gonotrophic cycle ($\tau_G(t)$), effects of age and temperature are indepen-

dent. The per capita mortality of adults in age class j is:

$$\delta_{A_j}(t) = \underbrace{h_j}_{\text{age effect}} \underbrace{\varphi_A T(t)^{\beta_A}}_{\text{temperature effect}} \quad (7)$$

for active adults and

$$\delta_{D_j}(t) = \begin{cases} h_j \varphi_A T(t)^{\beta_A} + \left(\frac{\Gamma}{\sqrt{2\pi\sigma^2}} \exp\left(-\frac{(t - \tau_G(t) - D)^2}{2\sigma^2}\right) \right), & \text{if } T(t) > \left(\frac{b_{da}}{h_j \varphi_A}\right)^{\frac{1}{\beta_A}}, \\ b_{da} + \left(\frac{\Gamma}{\sqrt{2\pi\sigma^2}} \exp\left(-\frac{(t - \tau_G(t) - D)^2}{2\sigma^2}\right) \right), & \text{otherwise,} \end{cases} \quad (8)$$

for diapausing adults, where $T(t)$ is the air temperature in $^{\circ}\text{C}$ on day t . For the range of temperatures that we explored in our simulations, $T(t)$ is non-negative. The function $\delta_{D_j}(t)$ is constrained to have a minimal value of b_{da} , corresponding to the essentially constant mortality rate of diapausing mosquitoes observed in the experiments from Bailey et al. (1982); Koenraadt et al. (2019). The expression of $\delta_{D_j}(t)$ (Eq. (8)) includes the post-diapause mortality that was introduced by Ewing et al. (2019). It accounts for the increased mortality that overwintered mosquitoes can experience (Hahn and Denlinger, 2007). We assume that mosquitoes in class $D_1(t)$ emerge from diapause at day $t = D$ and die after one gonotrophic cycle of length $\tau_G(t)$. The parameters σ and Γ are chosen so that overwintered mosquitoes are eliminated after emergence and egg-laying. The parametrisation of φ_A and β_A is based on the data from Ciota et al. (2014) and follows Ewing et al. (2016).

To determine the dependence of adult mortality on age, we compared 6 different models for h_j . Model selection (Appendix A.5) gave the best fit model to be

$$h_j = \kappa j^3, \quad 1 \leq j \leq N, \quad (9)$$

where κ is a positive constant and h_j describes the increasing adult mortality rate with age.

2.3. Egg-laying

Our model includes a description of the decrease in egg raft size with adult age (Roubaud, 1944; Awahmukalah and Brooks, 1985; Walter and Hacker, 1974). Studies have commonly described the effect of age (Awahmukalah and Brooks, 1985) or temperature (Madder et al., 1983) on fecundity, but rarely both. We assume that temperature only affects fecundity through the length of the gonotrophic cycle and use a general function describing how the egg raft size (ρ_j) depends on gonotrophic cycle number, j . For convenience, we assume that egg-laying is continuous during each gonotrophic cycle, which is a common modelling assumption (Caldwell et al., 2021; Brass et al., 2024). In particular, the continuous egg-laying assumption was successfully used in the model from Ewing et al. (2019). The birth rate is given by:

$$b_j(t) = \rho_j \zeta(t) / \tau_G(t) \quad (10)$$

where $\zeta(t)$ is the fraction of egg-laying adults at time t , given by

$$\zeta(t) = \begin{cases} \frac{1}{1 + \exp(\omega_{\text{spr}}(\xi_{\text{spr}} - \psi(t)))}, & \text{if } \text{mod}(t, 365) < 172.5, \\ \frac{1}{1 + \exp(\omega_{\text{aut}}(\xi_{\text{aut}} - \psi(t)))}, & \text{otherwise,} \end{cases} \quad (11)$$

where $\omega_{\text{spr}}, \xi_{\text{spr}}, \omega_{\text{aut}}, \xi_{\text{aut}}$ were parameterised by Ewing et al. (2019). The function $\zeta(t)$ reflects the fact that egg-laying activity by active female mosquitoes is driven by photoperiod. Hence, the number of active egg-laying adults is given by $\zeta(t) \sum_j A_j(t)$. The parameter ρ_j is the egg raft size of the adults in class $A_j(t)$. We also assume that overwintered mosquitoes produce the same egg raft size as those corresponding adults that have not overwintered, since current empirical data is inconclusive. While Madder et al. (1983) found evidence that overwintered

mosquitoes lay fewer eggs, Liu et al. (2016) did not observe such a clear pattern. Therefore, in spring, $D_1(t)$ adults have an egg raft size that is the same as $A_1(t)$ adults, namely ρ_1 and $\zeta(t)D_1(t)$ is the fraction of newly emerged $D_1(t)$ adults that are egg-laying in spring. The range of values for egg raft size that we explore in our model is based on the egg raft sizes observed by Madder et al. (1983). It is important to mention that in autumn, since individuals do not transition to diapause instantaneously, a fraction, $1 - \zeta(t)$, of adults are still active and not in diapause, but are no longer egg-laying. Formally, such individuals are not going through the gonotrophic cycles. Nonetheless, we assume that they age at exactly the same rate as they would age by going through the gonotrophic cycles.

Due to lack of data on the relationship between fecundity and age, we choose a general functional form to describe ρ_j as a decreasing function of j . We assume that after M gonotrophic cycles, egg raft size is zero and we denote by ρ_{avg} the average egg raft size of egg-laying adults across the gonotrophic cycles. For $j \leq M$, ρ_j is determined by:

$$\rho_j = \rho_{avg} \left[\alpha - (\theta + 1)(\alpha - 1) \left(\frac{j - 1}{M - 1} \right)^\theta \right], \quad (12)$$

where α determines how rapidly fecundity declines with age. A value of $\alpha = 1.5$ indicates that $A_1(t)$ lay 50% more eggs than the average ($\rho_1 = \alpha\rho_{avg}$). The parameter θ determines the concavity of Eq. (12) ($\theta = 1$, linear, $\theta < 1$, convex, $\theta > 1$, concave). The parameters θ , M , ρ_{avg} and α are constrained such that $\rho_j \geq 0$. Plots illustrating the shape of Eq. (12) are shown in Appendix A.6.

Empirical evidence for *Culex pipiens* has found that adults do not lay eggs after more than 6 gonotrophic cycles (Roubaud, 1944; Awah-mukalah and Brooks, 1985; Walter and Hacker, 1974). Therefore, we assume $M = 6$ for all our simulations. In Appendix B.1 we explored scenarios with $M > 6$ and illustrate that it does not have a significant effect on our results. To assess the effects of age-dependent egg-laying rates on mosquito abundance, we fix the average egg raft size to be $\rho_{avg} = 200$ (Ewing et al., 2019; Vinogradova, 2000). This allows us to isolate the effects of age of egg laying from the lifetime egg-laying potential of adults.

By fixing M and ρ_{avg} , the only free parameters are α and θ . In Appendix B.2 we illustrate that the effects of θ on adult abundances are small compared to the effects of α . Thus for the rest of the article, we keep $\theta = 1$ (Fig. A.13b) and focus our analysis on the effects of varying α . In particular, large values of α correspond to a strong effect of age on fecundity: an increased number of eggs being laid by younger adults and a smaller number of eggs laid by older adults (Fig. A.13b). At $\alpha = 1$, $\rho_1 = \rho_2 = \dots = \rho_M = \rho_{avg}$ and adults of all ages produce the same number of eggs, an egg raft size corresponding to ρ_{avg} . We refer to this case as age-independent fecundity.

2.4. Temperature profiles

To explore the effects of different temperature scenarios we run simulations using sinusoidal air temperature profiles (Fig. 2). We use North Kent Marshes in the UK as a reference location for temperature and photoperiod variations. It is known to be a common habitat for the *Culex* species complex, providing a realistic range of environmental conditions to which mosquitoes might be exposed and a likely location for the introduction of WNV into the UK (Golding et al., 2012; Vaux et al., 2015). The temperature function is given by

$$T(t) = \mu - \lambda + 2\lambda \left(\frac{1}{2} \left(1 + \cos \left(\frac{2\pi(t - (213 + \phi))}{365} \right) \right) \right)^\gamma. \quad (13)$$

The parameter μ denotes the mean annual temperature, λ the amplitude of the annual temperature, γ the length/sharpness of summer and ϕ the shift in timing of peak temperature, with the reference for the day of peak temperature being the 1st of August ($t = 213$). The choice of summer peak is consistent with the historic temperature recordings for North Kent Marshes (Hollis, 2017). We note that only when $\gamma = 1$ does μ directly correspond to the mean annual temperature. The water

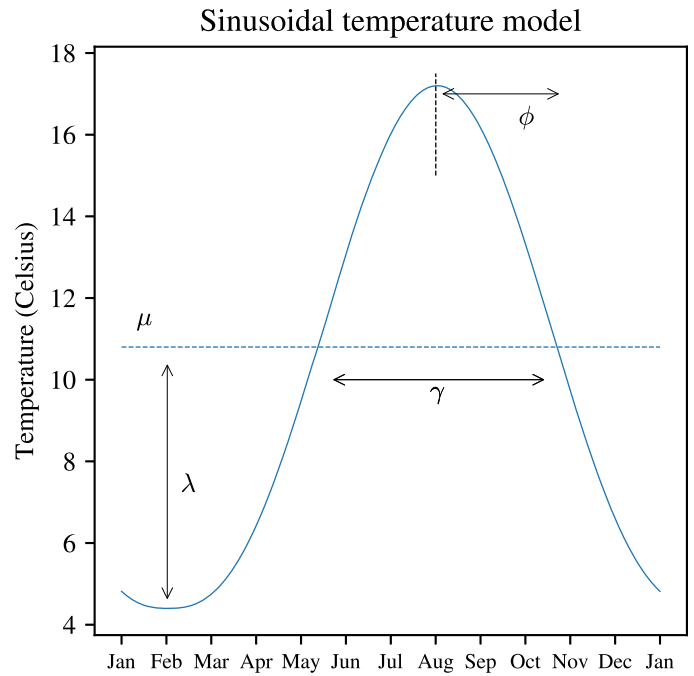


Fig. 2. Sinusoidal temperature profile, indicating the role of each parameter in Eq. (13). The parameters μ , λ , ϕ and γ denote mean temperature, temperature amplitude, timing of the peak summer temperature and length/sharpness of the summer season, respectively.

temperature that affects the immature stages is obtained from the air temperature using the regression performed by Ewing (2017):

$$T_{water} = 0.9491T_{air} + 3.9174. \quad (14)$$

We started the simulations following the procedure from Nisbet and Gurney (1983). Initially, all immature and adult populations being equal to 0 on the 1st of July ($t_0 = 183$). Then $J_0 = 100$ adults were inoculated into the $A_1(t)$ class for one day $\Delta t = 1$. Simulations were then run for 1.5 years under baseline conditions $\mu = 10.80$, $\lambda = 6.38$, $\phi = 0.55$, $\gamma = 1.25$ before changing the temperature to a specified scenario. The baseline temperature corresponds to a least mean squares fit of Eq. (13) to the mean daily temperature time series from Hollis (2017) at the grid point nearest to North Kent Marshes (approximately (latitude, longitude) = (51° 29', 0° 30')) from 1960 to 1990. Subsequently simulations were run for different values of μ , λ , ϕ , γ to assess the effects of alternative temperature scenarios on mosquito abundances. Each simulation was run for enough time for transient effects to be negligible for our results. The range of μ , λ , ϕ and γ explored is based on the maximum and minimum values of such parameters across every year of the time series from North Kent marshes from the 1960–1990 period (Hollis, 2017).

In addition to temperature values based on historical time series from the Kent Marshes, we also use estimates of future climate parameters based on the UK Climate Projections (Met Office Hadley Centre, 2018). The climate projections considered are the following:

1. Average emission scenario (RCP 4.5) for 2020s, 2050s and 2080s in the Southeast of England (where the North Kent Marshes are located). The RCP 4.5 projection uses the 1960–90 data as a baseline for the estimates of future mean (μ) and maximum/minimum (λ) temperature estimates. Since there were no RCP 4.5 predictions for ϕ , γ , unless otherwise specified, ϕ , γ values are kept at the 1960–90 as a baseline values ($\phi = 0.55$, $\gamma = 1.25$). The RCP 4.5 scenarios are used in Section 3.2 and Section 3.3 and Appendix B.2 and Appendix B.6.
2. High emission scenario (RCP 8.5) for the periods of 2010–2029, 2030–2049 and 2050–2069 for the North Kent Marshes, which we refer to as 2020s, 2040s and 2060s, respectively. The RCP

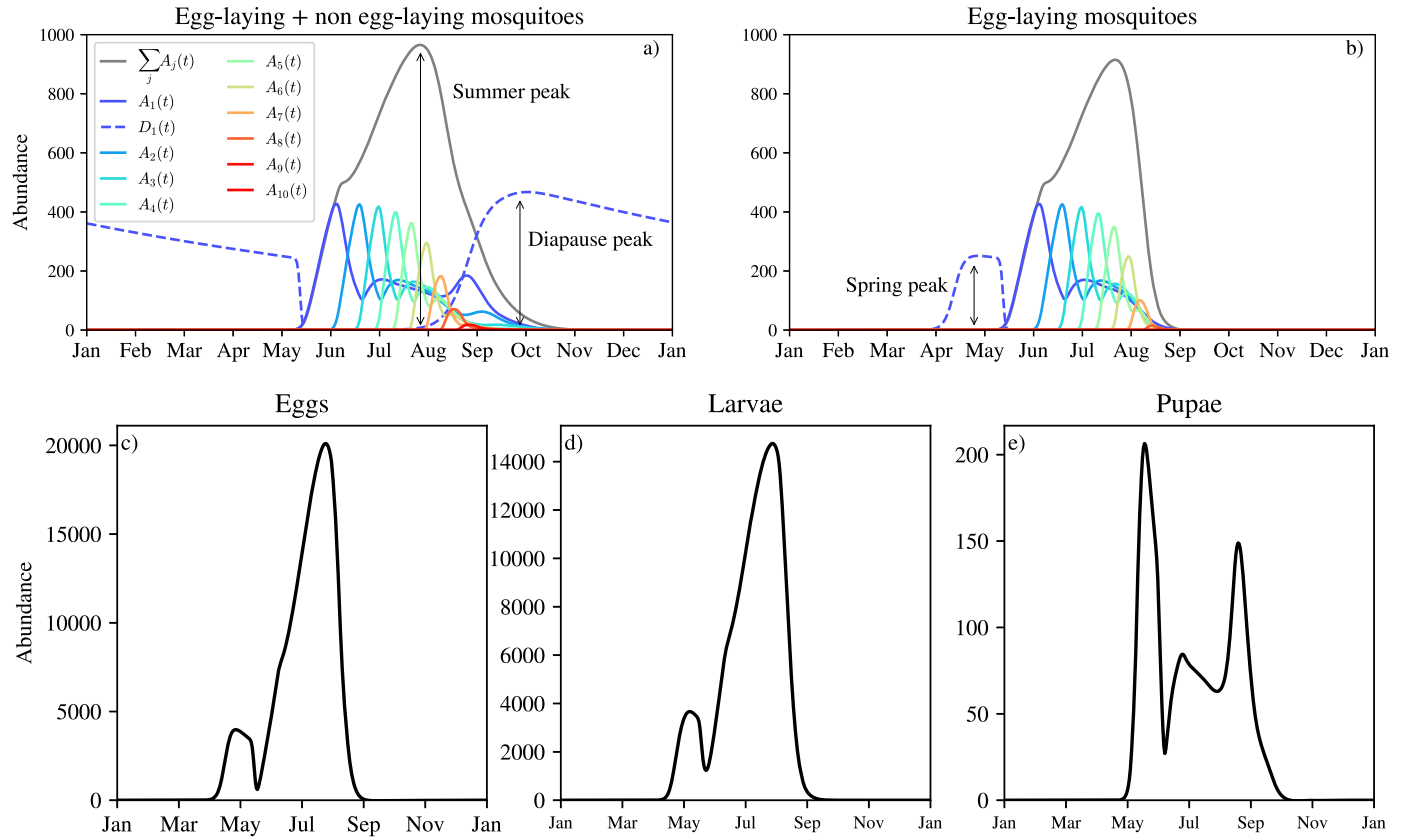


Fig. 3. Mosquito abundance profiles following an initial burn-in of 5 years. (a) Active ($A_j(t)$) (blue to red coloured lines) and diapausing ($D_1(t)$) (blue dashed lines) adult mosquitoes. The grey line corresponds to the total abundance of active adults ($\sum_j A_j(t)$). (b) egg-laying active adults ($\zeta(t)A_j(t)$, continuous lines) and egg-laying post-diapausing adults ($\zeta(t)D_1(t)$, dashed lines). The grey line corresponds to $\zeta(t)\sum_j A_j(t)$, the total abundance of egg-laying active adults. We simulate with $N = 10$ adult classes that lay eggs until class $M = 6$. (c)–(e) Immature population abundances. Temperature parameters are taken from the 1960–90 historical recordings: $\mu = 10.80$, $\lambda = 6.38$, $\phi = 0.55$, $\gamma = 1.25$. Egg-laying is taken to be independent of age, that is, $\alpha = 1.0$. In this simulation and throughout the rest of the results we use $N = 10$ adult classes and $M = 6$ egg-laying adult classes.

8.5 projections are average daily temperatures and can therefore be used to obtain estimates of not only μ, λ , but also ϕ, γ , using least squares fitting of the temperature time series. The RCP 8.5 temperature dataset consists of 12 stochastic runs. We select 4 runs out of the 12 (runs 1, 5, 7, 10) that lead to typical (excluding outliers) temperature parameter predictions to illustrate general temperature trends. However, our conclusions remain consistent with the predictions of the remaining runs. When indicating the future temperature projections on Fig. 8, (μ, λ) are obtained from fits of Eq. (13) to the climate projection data while fixing (ϕ, γ) to values taken from baseline historical records. In Fig. 9 we proceed in a similar fashion, but instead fixing (μ, λ) and fitting (ϕ, γ) . RCP 8.5 projections are used in Section 3.4.

To complete the description of the model, the history functions are given in Appendix A.7. The table of all model parameters can be found in Appendix A.8. Parameters take the values in Tables A.2 and A.3 unless otherwise stated. All simulations are run using the Differential Equations library from Julia. Specifically, we use the DDE solver with the Method of Steps (Driver, 2012) with a relative and absolute tolerances of 10^{-10} . The code used in our simulations is available at Andrade et al. (2025).

3. Results

Fig. 3 illustrates typical abundance profiles obtained from the model. In the simulation shown in Fig. 3 and throughout the rest of the results we use $N = 10$ adult classes and $M = 6$ egg-laying adult classes unless

explicitly specified otherwise. To facilitate the discussion of the results, we define the *summer peak abundance* to be the maximum value of active adults ($\sum_j A_j(t)$) over the last year of the simulations, and define the *diapausing peak abundance*, to be the corresponding maximum value of $D_1(t)$ (Fig. 3a). The *spring peak* is defined as the maximum value of $\zeta(t)D_1(t)$. The $D_1(t)$ adults are only egg-laying once they have emerged from diapause in spring and $\zeta(t)$ determines the fraction of emerged $D_1(t)$ adults (see Fig. 3b).

The height of the spring peak is determined by the height of the diapause peak since overwinter mortality occurs at an approximately constant rate (Koenraadt et al., 2019). Therefore, changes in the number of mosquitoes emerging in spring reflects changes in the peak number of mosquitoes in diapause. We choose to focus our analysis on the diapausing peak instead of the spring peak since the latter depends on the egg-laying activity function $\zeta(t)$, which relies on assumptions about the cues for entering and leaving diapause. The diapausing peak provides a more general description of the size of the maximum overwintering population and a proxy measure for the size of the spring peak.

3.1. Assessing the impact of age-dependent diapause survival

Based on the empirical observation that only nulliparous diapausing adults survive winter, we assumed only the $D_1(t)$ diapausing adults can contribute to the adult population and egg-laying pool in spring. In this section, we examine the impact of this age-dependent diapause survival on the spring abundance profile. In Fig. 4, the continuous lines

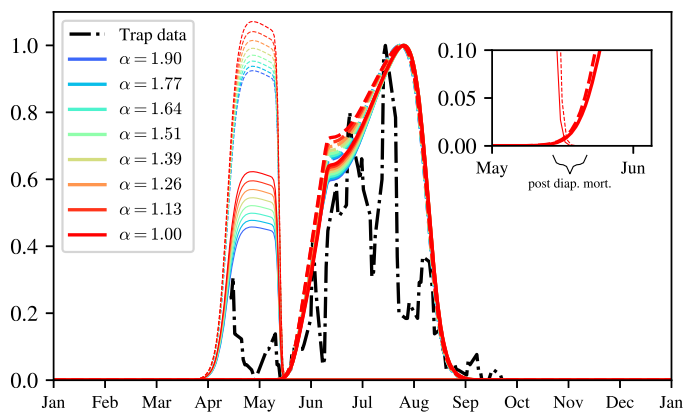


Fig. 4. Comparison between egg-laying adult abundances from the model using a sinusoidal temperature profile and normalised 3-day averaged trap data from Ewing et al. (2019). The dashed lines represent simulations where all $D_j(t)$ classes survive overwinter and the continuous lines when only $D_1(t)$ survives overwinter. Thicker lines: total number of egg-laying active adults ($\sum_j \zeta(t)A_j(t)$). Thinner lines: dashed lines indicate total egg-laying post-diapause adults ($\sum_j \zeta(t)D_j(t)$), the solid line indicates only post-diapausing egg-laying adults of the first adult class ($\zeta(t)D_1(t)$). For each curve, adult abundances are normalised with respect to the corresponding summer peak abundances. Temperatures were fitted to the hourly-recorded air temperature data from Ewing et al. (2019) using the model described in Eq. (13): ($\mu, \lambda, \phi, \gamma = 11.41, 5.41, 9.47, 1.68$). In the simulation runs corresponding to the dashed lines, all adults survive diapause irrespective of their age, as done by Ewing et al. (2019).

correspond to the case in which only the $D_1(t)$ class survives overwinter and therefore contributes to the population in the spring of the following year. Conversely, the dashed lines correspond to the case in which all diapausing classes ($D_j(t)$) survive overwinter and lay eggs in spring. We compare these two cases to the 3-day averaged trap data from Ewing et al. (2019) (black dashed-dot line). In each case, adult abundances are normalised with respect to the summer peak in that year to allow comparisons between the simulations and the trap data. The results from Fig. 4 illustrate how allowing only younger adults to survive overwinter combined with the age-dependent fecundity can help explain the small size of the spring peak, a feature that was not fully described by the model presented by Ewing et al. (2019).

In Ewing et al. (2019), simulations used hourly temperature data, resulting in temperature fluctuations not captured by the sinusoidal seasonal temperature profiles used in our model, limiting direct comparisons between our simulations and the simulations from Ewing et al. (2019). Hence to understand the role senescence and overwintering survival in Fig. 4, we compare our model outputs to the trap data from Ewing et al. (2019), with sinusoidal temperatures fit to the hourly temperature recordings from Ewing et al. (2019). By tracking active adults and diapausing adults separately we can more accurately capture spring mortality. Ewing et al. (2019) consider a single adult class, making no distinction between newly emerged active adults in spring and post-diapause adults. A closer look at the population curves around mid-May (Fig. 4, inset) shows that there are adult offspring of post-diapause adults that are present before the $D_1(t)$ adults have died. However, in the Ewing et al. (2019) model, post-diapause spring mortality kills both of overwintered individuals and their offspring, when in fact only the overwintered individuals should die. We illustrate this remark for the temperature parameters fitted to Ewing et al. (2019), but it is even more pronounced for simulations carried out at higher temperatures or when summers are warmer and earlier (higher μ 's and smaller ϕ 's, respectively, not shown). This early death of the $A_j(t)$ adults in spring can lead to an underestimation of the summer peak in the Ewing et al. (2019) model and further contributes to the mismatch between trap data and model predictions observed by Ewing et al. (2019).

3.2. The role of age-dependent mortality in the context of age-dependent fecundity

In this section we compare adult abundances from the model with age-dependent adult mortality to the model with age-independent mortality, while also varying how rapidly fecundity declines with age (α). Fig. 5 demonstrates that adult abundance at both summer and diapause peaks is higher when adult mortality is age-dependent compared to when adult mortality is age-independent. The higher peak abundances observed with the age-dependent mortality model are illustrated by the positive values in Fig. 5a and b, that indicate the difference in the peak size between the two model variants. The lower mortality of younger adults in the age-dependent case facilitates population growth and explains the higher abundances.

Increasing the rate at which fecundity declines with age (increasing α) impacts peak mosquito abundance in the age-dependent and the age-independent mortality models differently. In most instances, increasing α increases the peak abundances both when adult mortality is age-dependent and when it is age-independent. However, when temperatures are sufficiently high, as in the 2080s RCP 4.5 projections and mortality is age-dependent, the declining fecundity with age can start to have a negative impact on population peak abundance, as observed in Fig. 5c for $\alpha > 1.4$. In the age-dependent mortality scenario, if fecundity decreases rapidly with age (high α), young adults have both a low mortality and high fecundity, but for sufficiently high α the net effect is a decline in overall population abundance. The decline is due high larval competition as a result of the large larval population. The high larval mortality via competition then results in a decline in the adult population. For smaller α , the strength of larval competition is lower and the decline in the adult population is not observed (see Fig. 5c for $\alpha < 1.4$). We further discuss the adult abundance decline due to larval competition in Section 3.3.

3.3. The limiting effect of larval competition on adult summer peak abundance

In this section we explore how larval competition can limit the adult abundance at the summer peak when both temperatures are high and fecundity declines rapidly with age (high α). Firstly, we examine the impact of varying only the rate at which fecundity declines with age (α) on larval competition. Secondly, we show how increased values of α combined with high temperatures lead to decreased adult abundances through larval competition.

In Fig. 6a–c, we plot the contribution of each adult age class to the population egg-laying rate across the egg-laying season, illustrating a shift in the relative contribution of the adult class to the immature stages. By comparing the plots in Fig. 6a–c, we observe that as α is increased, young adults contribute a greater fraction of the total egg-laying, as shown by the increase in size of the blue and green areas when comparing plot b to a and plot c to b. In fact, by integrating over the whole season, the eggs laid by $A_1(t)$ adults shift from 24.9% of the total number of eggs laid when $\alpha = 1.0$ to 32.2% when $\alpha = 1.9$. The increase in eggs laid by young adults as we increase α happens since increasing α means that younger adults have larger egg raft sizes than older adults. It is worth mentioning that the increase in eggs laid by young adults happens despite the relative contribution of young adults to the total population not changing significantly as we change α (shown in Appendix B.4), and thus the increase in egg-laying by young adults is not caused by an increase in the relative abundance of young adults. Since the young adults are naturally the first ones to emerge in spring, they compose the majority of the adult population early in the season. As a result, the increase in eggs laid by young adults obtained from increasing α leads to an increased egg-laying rate early in the season, as can be seen by comparing the blue shaded areas in Fig. 6a–c. When α is high, the increased egg-laying rate early in the season leads to an accumulation of eggs laid within a shorter time frame, as opposed to eggs being

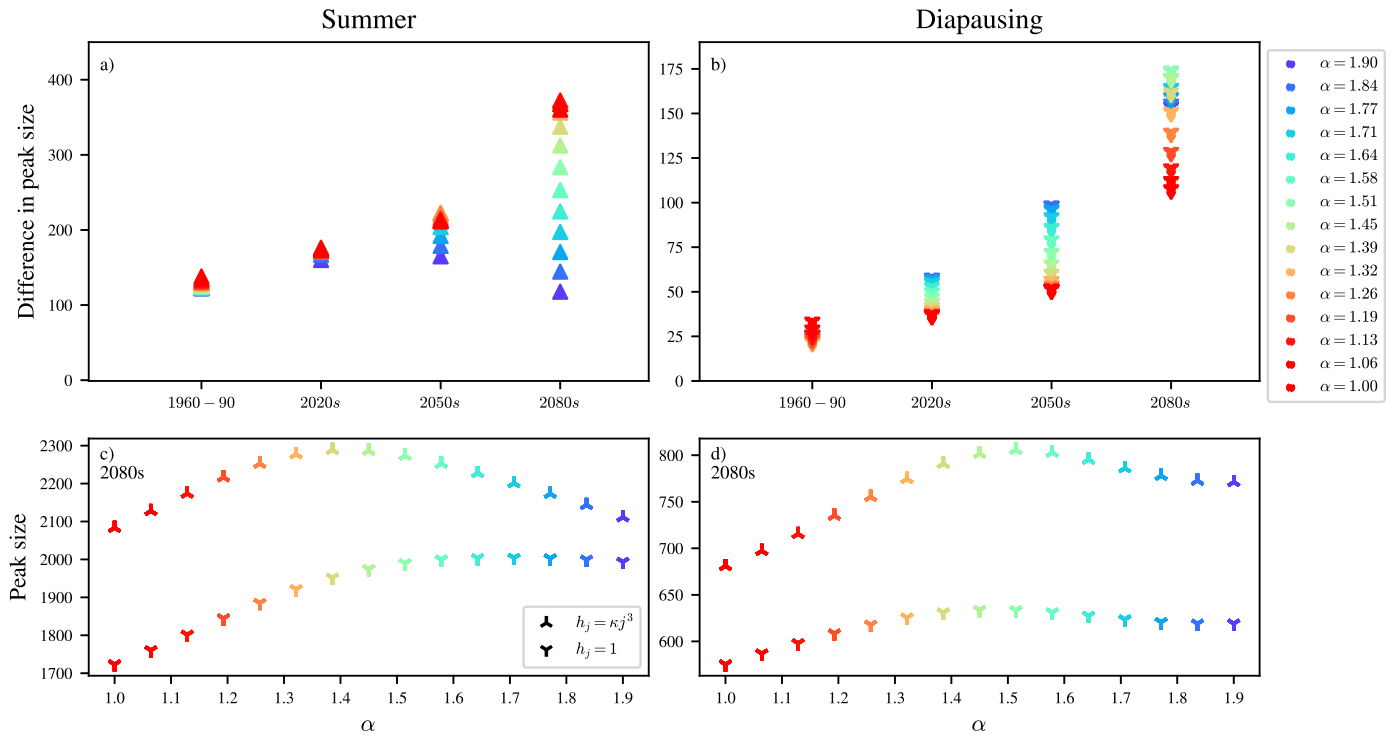


Fig. 5. Comparing two model variants, one in which mortality is age-dependent ($h_j = \kappa j^3$), the other in which mortality is age-independent ($h_j = 1.0$), while also varying the rate at which fecundity decreases with age (α). The last year of 7 years of simulations is considered for all plots. Different colours correspond to different values of α , as indicated in the legend. (a) Difference in adult summer peak size between model variants when adult mortality is age-dependent versus age-independent, under four temperature scenarios (1960–1990 daily temperatures and RCP 4.5 projections for 2020s, 2050s and 2080s). (b) Analogous to (a), comparing adult diapausing peaks. (c,d) Summer and diapause peak values as function of α , comparing the case of age-dependent mortality to the case of age-independent mortality, under temperature scenario RCP 4.5 - 2080.

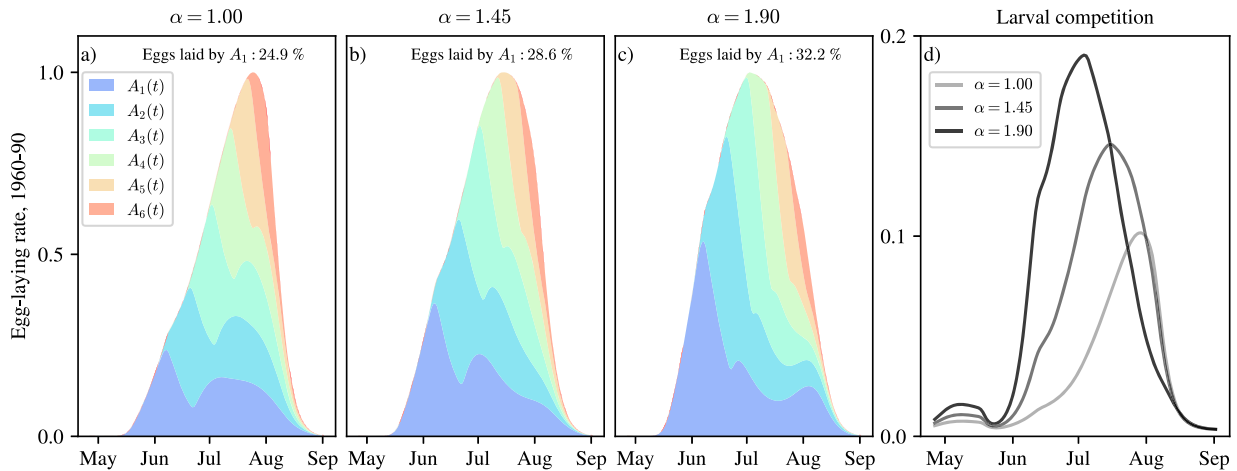


Fig. 6. The effect of α (the rate at which fecundity decreases with age) on the egg-laying rate of each adult class and larval competition. (a–c) Stack plot of the total egg-laying rate ($\zeta(t)A_j(t)\rho_j/\tau_G(t)$, $j = 1, 2, \dots, M$) for each $A_j(t)$ adult class for three different values of α . Annotations indicate the percentage of eggs laid by $A_1(t)$ over the duration of egg-laying season, obtained through numerical integration. Plots are of normalised rates over the last year of 7 years of simulations. (d) Larval density-dependent mortality due to competition in days⁻¹ for three different values of α . For (a–d) temperature parameters are $(\mu, \lambda, \phi, \gamma) = (10.80, 6.38, 0.55, 1.25)$, estimated from the 1960–90 historical records.

laid more evenly across the season when α is small. After hatching, the eggs accumulated early in the season culminate in a concentrated peak of larvae, that results in high larval competition. In Fig. 6d we illustrate how larval mortality due to competition increases as we increase α . Moreover, in Fig. 6d we observe that the peak in larval mortality due to competition also shifts to earlier in the season we increase α , further indicating the shift in larval abundances towards earlier in the season.

To complete the picture, we now illustrate how the effects of age-dependent fecundity on larval competition are amplified by high tem-

peratures. In Fig. 7, we plot the (a) larval peak and (b) adult summer peak abundances as functions of α for different temperature scenarios. In all temperature scenarios, we observe that larval abundance peaks increase if α is increased enough (Fig. 7a). Overall, the adult summer peaks also increase with α (Fig. 7b), despite the increased larval competition associated to high α . However, if temperatures are increased to the RCP 4.5 2080s projections (red curve in Fig. 7b), we observe that adult abundance peaks decrease for $\alpha > 1.4$. The decrease in adult abundance happens due to the increased larval competition that was

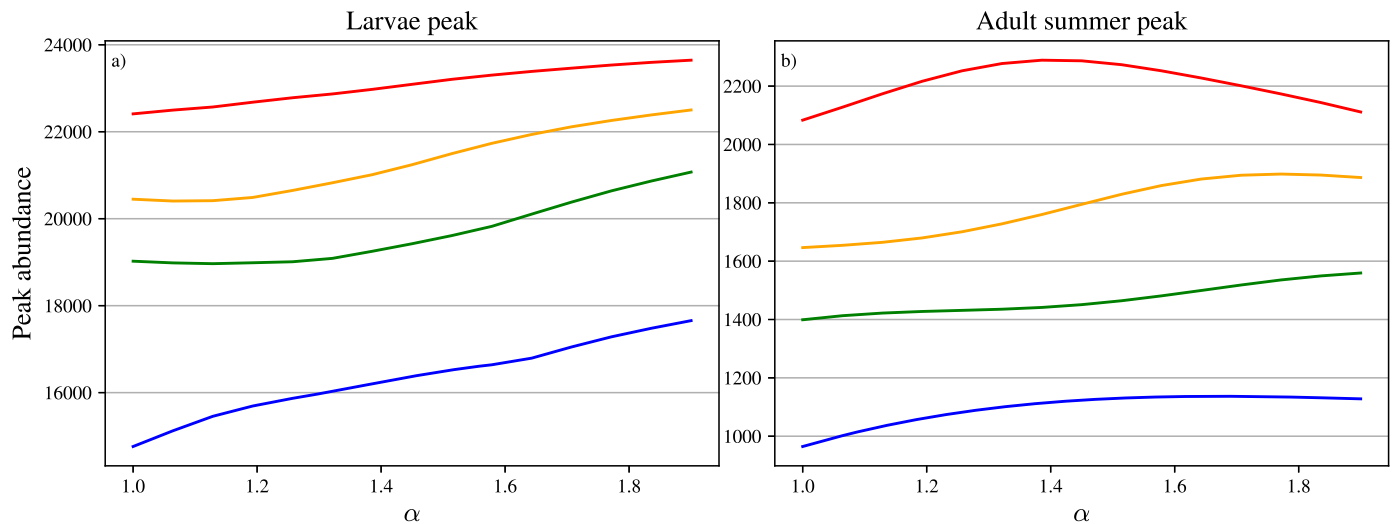


Fig. 7. Size of the (a) larval and (b) summer adult peaks in abundance plotted as functions of α , the rate at which fecundity declines with age. Each plot illustrates four temperature scenarios: 1960–90 daily temperatures (blue) and RCP 4.5 temperature projections for 2020s (green), 2050s (orange) and 2080s (red).

illustrated in Fig. 6d and that is amplified by the increased abundances in high temperatures. Therefore, when both temperatures are high and fecundity decreases rapidly with age, larval abundance and hence larval competition are increased sufficiently that the rise in the size of the larval abundance peak is not carried through to a similar rise in the adult summer abundance peak. In Appendix B.6 we further discuss larval mortality due to competition under different temperature scenarios. In particular, we demonstrate that changes in α do not significantly affect the larval mortality due to predation and thus the increased larval mortality we observe with high α is only due to competition.

3.4. Exploring the effects of temperature via μ , λ , ϕ , γ

In this section we explore the response of mosquito population dynamics to changes not only to mean temperature (μ) and temperature amplitude (λ), but also to timing (ϕ) and length of the summer (γ). By considering the range of μ , λ , ϕ , γ based on historical recordings from 1960 to 90 (Hollis, 2017) we explore how different properties of the temperature profile affect peak abundances, a similar approach as Ewing et al. (2016). The range of each temperature parameter is determined individually by fitting Eq. (13) to the historical recordings to each year from 1960 to 90. Estimates of μ , λ , ϕ and γ from temperature time series often show considerable correlation (Ewing et al., 2016), so as reference points for discussion, we indicate the RCP 8.5 (high emissions scenario) predictions for μ , λ on plots in Fig. 8 and for ϕ , γ on plots in Fig. 9. We consider the high emission scenario as this is the only scenario where daily temperature predictions are available, necessary to estimate timing (ϕ) and length of summer (γ), as explained in Section 2.4.

Initially, we explore the effects of varying μ and λ while fixing ϕ and γ at the fitted values for the whole 1960–90 period. In Fig. 8 heatmaps of adult abundance at summer peaks and diapause peaks are plotted as functions of μ , λ , for three different values of α , corresponding to different rates in which fecundity decreases with adult age. Overall, we observe that for all values of α , both summer and diapause peaks tend to increase in size with respect to μ and λ . Notably, μ has a more visible effect than λ , as suggested by the close to vertical level curves, especially in Fig. 8a–c. The climate predictions obtained from the RCP 8.5 data (Met Office Hadley Centre, 2018) are illustrated by the markers on the heat maps in Fig. 8 and show that the model suggests peak adult abundance (summer and diapause) is expected to increase over the next century.

Moreover, by comparing Fig. 8a–c for lower and intermediate mean temperature values ($\mu \leq 14$), we observe that age-dependent fecundity ($\alpha = 1.375$, $\alpha = 1.75$) can result in slightly higher peaks in adult abundance compared to when fecundity is independent of adult age ($\alpha = 1.0$). For example, compare the position of the 1800 level curve with respect to the location of the climate projection markers around $\mu = 13$ in each plot (Fig. 8a–c). However, for higher values of mean temperature ($\mu > 14$), $\alpha = 1.0$ gives rise to a higher summer peak than $\alpha = 1.75$, due to the increased larval competition that can result from age-dependent fecundity, as discussed in Section 3.3.

We additionally consider the effects of changing timing (ϕ) and summer duration (γ) while keeping the mean temperature (μ) and temperature amplitude (λ) fixed at the 1960–90 values. By comparing plots in Fig. 9a–c, we observe that the size of the summer peak tends to increase as we allow fecundity to decline more rapidly with age (increasing α). A similar pattern holds for the adult abundance at the diapausing peak (Fig. 9d–f).

We observe that summer peaks in adult abundance (Fig. 9a–c) tend to be higher when summer is longer (small γ). Similar to our discussion in Section 3.3, the warmer temperatures due to the longer summers cause the younger adults to lay proportionally more eggs than older adults, especially when α is high (> 1.0), leading to an overall increase in peak abundances. If the summers are earlier ($\phi < 0$), the egg-laying of younger adults, which are more abundant earlier in the season (Fig. B.16), is also increased, leading to similar increases to summer peak abundance to those seen when summer is longer (small γ).

The heatmaps of the diapause peak abundances (Fig. 9d–f) differ from the heatmaps of the summer peak abundances in their response to ϕ and γ . The most striking difference is that the size of diapause abundance peaks are highest at intermediate values of γ and ϕ . First, we focus on the effect of varying γ . For high values of γ (short summers), the period of high temperatures is small, resulting in lower adult abundances. For low values of γ (long summers), the diapause peak is also smaller than observed under the 1960–90 reference temperature (\circ markers), despite a larger peak in summer abundances. The cause of the smaller diapause peak is due to a shift in the active adult age distribution towards older adults (Appendix B.4), caused by a shorter gonotrophic cycle and faster aging associated to the long periods of warm temperatures when γ is small. When the adult population enters diapause, fewer individuals are young adults and only $D_1(t)$ adults survive winter and are considered in the diapause peak. It is important to note that the shift in age composition also happens by increasing the mean temperature

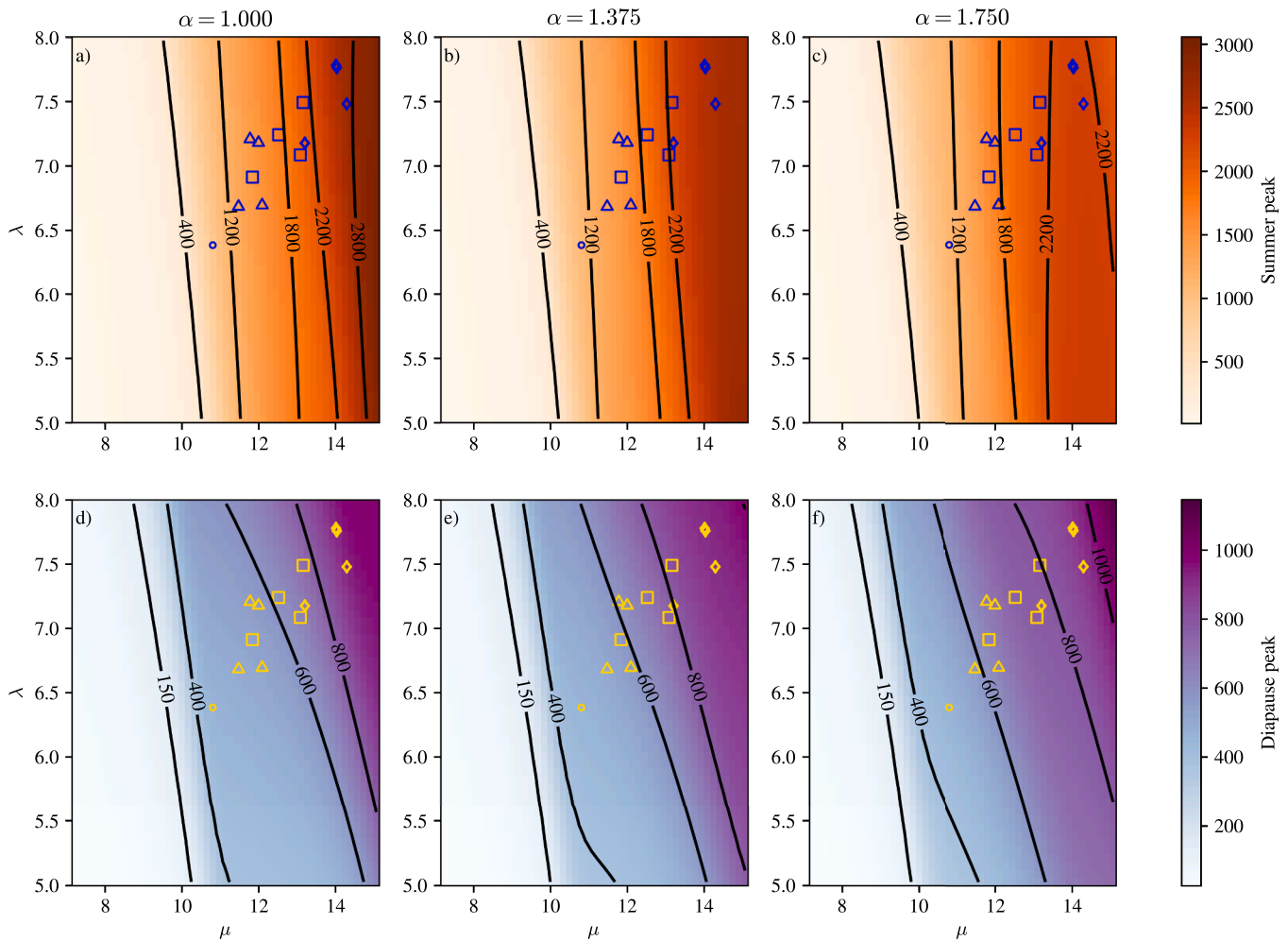


Fig. 8. Heatmaps for adult abundance at summer peaks (a–c) and diapause peaks (d–f) over one year following an initial burn-in of 5 years for different values μ , λ , and fixed $(\phi, \gamma) = (0.55, 1.25)$, taken from 1960 to 90 daily temperatures. Circles (o) represent the baseline μ , λ for 1960–90 historic values (Hollis, 2017). The other markers indicate the predicted values of μ , λ according to the daily temperature climate projections for 2020s (Δ), 2040s (\square), 2060s (\diamond) for 4 different runs under RCP 8.5 (Met Office Hadley Centre, 2018). The fitting of μ , λ for the climate projections are made with fixed ϕ , γ for consistency to the rest of the heatmap. In column 1, adult fecundity is independent of adult age ($\alpha = 1.0$), while in columns 2 and 3 adult fecundity declines with age, with higher values of α corresponding to a steeper relationship between age and fecundity. Adult mortality increases with age according to $h_j = \kappa j^3$.

(μ , Fig. 8), as shown in Appendix B.4. However, when μ is high, summer abundances are increased enough to cause $D_1(t)$ abundances to increase, despite the adult population being older. Therefore, the decrease in the diapause peak abundances for small values of γ is only observed when μ is fixed at a sufficiently low value.

The effect of varying the timing of the summer (ϕ) on the diapause abundance peaks (Fig. 9d–f) depends on the length of summer (γ). The effect of later summers (positive ϕ) are mostly seen when summers are long. For high γ 's, positive ϕ 's further decrease the size of the diapause abundance peak by moving the short summers towards the end of activity season. Analogously, the effect of earlier summers (negative ϕ) are mainly observed at small values of γ . The long summers, that are shifted earlier when ϕ is negative, also shift adult abundance peaks towards earlier in the year, leading to fewer young adults late in the season that later go on to constitute the diapause abundance peak (composed only of $D_1(t)$).

The RCP 8.5 climate projections for ϕ do not follow a clear decadal trend (Fig. 9). In contrast, the climate projections for γ suggest an increase in the length of summer (smaller γ) when compared to the historical recordings (o). Therefore, under RCP 8.5 climate projections, our model predicts overall higher summer peaks in adult abundances, in spite of also predicting slightly smaller values of the diapause (and hence, spring) peaks.

4. Discussion

In the face of climate change, while VBDs are already a significant public health issue in many regions, there is an increased risk of emergence of VBDs in areas where they were previously absent (Rogers and Randolph, 2006; Caminade et al., 2019; Wilson et al., 2020). Mosquitoes are amongst the most important vectors of VBDs (Organization, 2022; Franklin et al., 2019; Manguin and Boète, 2011), and hence it is imperative to understand the interplay of factors shaping their population dynamics in order to effectively assess the risks of future VBD outbreaks. The dynamics of mosquitoes are influenced by multiple abiotic and biotic factors. Of these factors, senescence has been increasingly recognised as having a role to play in VBD transmission (Pigeault et al., 2015; Knecht et al., 2018; Johnson et al., 2020; Somé et al., 2024). Despite the known effects of temperature and age on mosquito biology, few studies have considered their combined impact on mosquito abundance. A detailed description of temperature effects on mosquito development rates and age effects on adult fecundity was previously explored by Lončarić and Hackenberger (2013) through an age-structured, discrete-time matrix model. Using a different framework (DDEs), our study distinguishes itself by incorporating not only age effects on adult fecundity, but also on adult mortality, while keeping the temperature-dependent effects on mosquito maturation and mortality as described by Ewing et al. (2019).

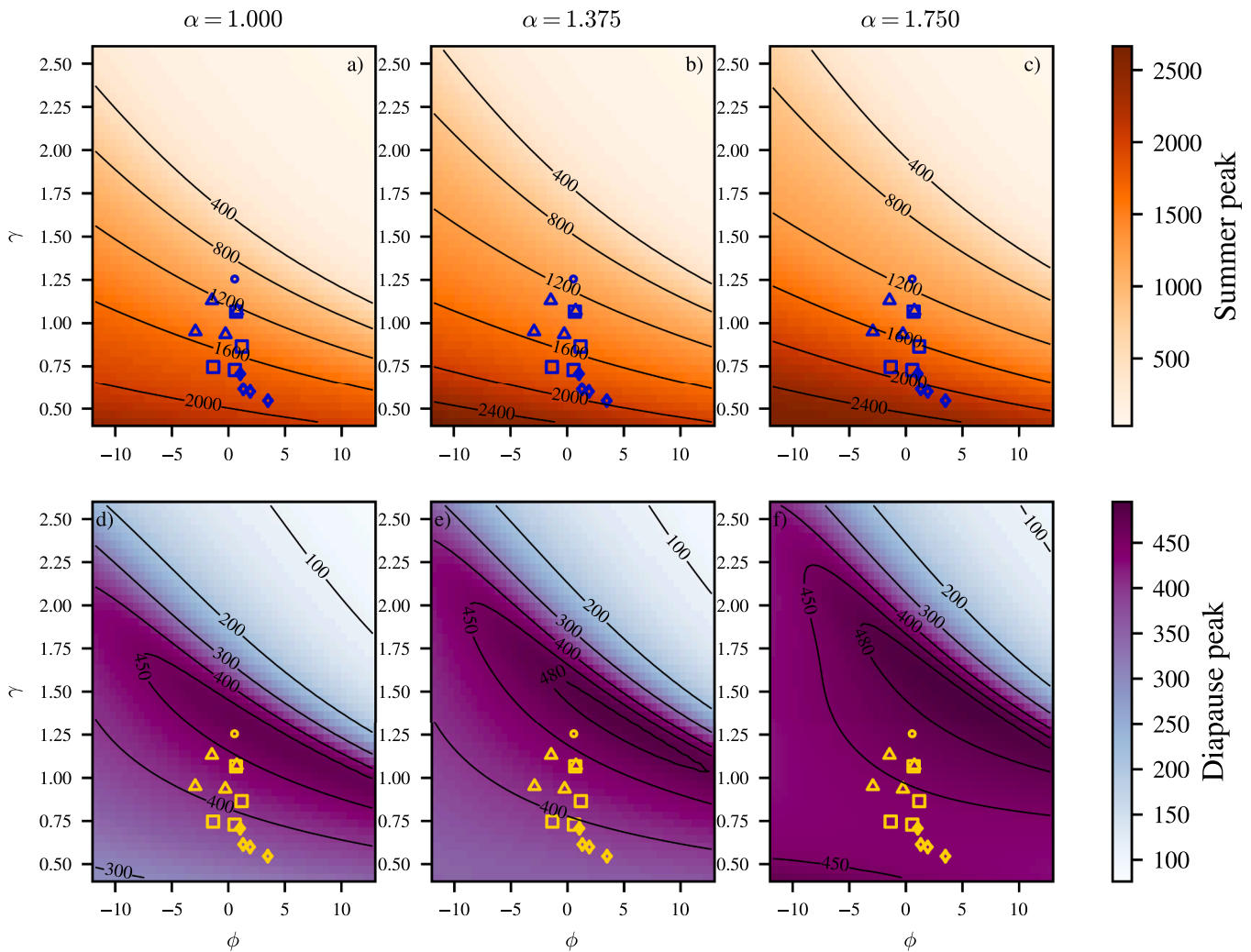


Fig. 9. Heatmaps for adult abundance at the summer peaks (a–c) and diapause peaks (d–f) over one year following an initial burn-in of 5 years for different values of the timing (ϕ) and length of summer (γ), and fixed $(\mu, \lambda) = (10.80, 6.38)$, taken from 1960 to 90 daily temperatures. Circles (\circ) represent the baseline ϕ, γ for 1960–90 historic values (Hollis, 2017). The other markers indicate the predicted values of ϕ, γ according to the daily temperature RCP 8.5 climate projections for 2020s (\triangle), 2040s (\square), 2060s (\diamond) for fixed μ, λ and for 4 different runs under RCP 8.5 (Met Office Hadley Centre, 2018). In column 1, adult fecundity is independent of adult age ($\alpha = 1.0$), while in columns 2 and 3 adult fecundity declines with age, with higher values of α corresponding to a steeper relationship between age and fecundity. Adult mortality increases with age according to $h_j = \kappa j^3$.

We aim to elucidate the role of senescence in shaping mosquito abundance and dynamics under changing temperature scenarios.

We have extended the temperature-dependent DDE model of the mosquito life cycle from Ewing et al. (2019) by incorporating the effects of age on adult fecundity and mortality. Our work uses the number of gonotrophic cycles experienced by adults as a proxy for adult age, an approach that can be applied to many mosquito species. An unexpected insight from the modelling revealed that including age-dependent adult mortality can lead to higher adult abundances than when mortality does not vary with age. Age dependent mortality associates high mortality to older adults, but also low mortality to younger adults. Since younger mosquitoes constitute the majority of the adult population when the entire activity season is considered, overall adult mosquito mortality is lower when mortality is age dependent than when it is age independent. Hence failing to consider mosquito senescence may underestimate the expected increase in mosquito abundances under increasing temperature scenarios. Our results depend significantly on young adults having a lower mortality than older adults and are, therefore, in line with previous empirical studies that highlight the importance of considering age structure in estimating mosquito abundances (Styer et al., 2007a,b; Harrington et al., 2014). Moreover, since the mortality rate can vary

significantly within a mosquito population, neglecting the age effects on mosquito mortality can hamper accurate estimates of the survival rates of mosquito populations and overestimate the efficacy of control strategies, as discussed by (Bellan, 2010).

Our model was able to assess the effects of hypothetical temperature profiles, based on both historical values for North Kent Marshes and future climate projections, on adult abundances. Warmer summers tend to increase the size of both summer and diapause peaks. As expected from temperate ectotherms, our results suggest that *Cx. pipiens* in North Kent Marshes are likely to experience increased abundances under increased temperatures (Deutsch et al., 2008; Ewing et al., 2016). Increases in mosquito abundance can in turn increase risks of MBD outbreaks (Semenza and Suk, 2018), including into previously unaffected regions (El-Sayed and Kamel, 2020; Chala and Hamde, 2021). However, if fecundity decreases rapidly with age and temperatures are high, towards the extremes predicted by future climate change scenarios, we find adult mosquito abundance begins to decline. The decline in adult abundances is caused by increased larval competition at these extreme temperatures. The detrimental effects of extreme temperatures on ectotherms has been previously discussed in the literature (Deutsch et al., 2008; Mohammed and Chadee, 2011). Amarasekare and Coutinho (2014)

explored the role that competition has on life-history traits of ectotherms, indicating how mortality due to intraspecific competition can play an important part in causing abundances at high temperatures to decrease. In turn, our work suggests that the effects of age on mosquito populations can accentuate mortality via competition, particularly at high temperatures. The fact the age-dependent mechanisms can shape ranges of temperature in which adult populations are expected to increase or decrease underscores the importance of senescence to accurately describe mosquito population dynamics. Furthermore, our results align with the established literature on the crucial role of larval competition in regulating adult mosquito abundances (Agnew et al., 2000; Tsurim et al., 2013), while also indicating how age-dependent mortality and fecundity can intensify these regulatory effects.

Introducing explicit adult age structure into the model also allowed insights into mosquito overwintering and spring abundances. Empirical studies provide evidence that the mosquitoes which survive winter are mostly nulliparous (Jaenson, 1987; Vinogradova, 2000). By including this observation into the model through only allowing adults in their first gonotrophic cycle to survive winter, we found that the size of the spring peak in adult abundance was smaller than when allowing diapausing adults of all ages to survive winter. The smaller spring peak is consistent with field observations (Ewing et al., 2019) and supports the hypothesis of Ewing et al. (2019) that argues that the age structure of overwintering adults plays a role in explaining spring peak size.

Our results also suggest that under longer and earlier summers, the proportion of younger adults in the active population can decrease as a result of the rapid aging and short gonotrophic cycle length associated with warmer temperatures. If the mean annual temperatures are not significantly increased, the reduction in the proportion of young adults in the population caused by longer and earlier summers leads to smaller spring peaks, as adults tend to be older when they enter diapause and are unable to survive winter. The recent development of new mosquito-age grading techniques (Siria et al., 2022) offers an opportunity to test this hypothesis by comparing the proportion of young adults between locations with different temperature profiles. Moreover, the shifts in the age composition of a mosquito population are expected to have implications for disease, given that adult mosquito age is known to affect vectorial capacity for several MBDs (Johnson et al., 2020). Previous modelling studies (Styer et al., 2007b; Bellan, 2010; Rock et al., 2015) have argued that younger adult mosquitoes have a disproportionately more important role in the transmission of MBDs, due to a higher chance of young mosquitoes surviving the extrinsic incubation period and hence going on to transmit disease. Nonetheless, MBD dynamics are likely to be nuanced, with increased temperatures expected to increase mosquito abundances, but decrease the proportion of young adults that might drive disease spread, leaving potential for both increases and decreases in MBD. We argue that further empirical and modelling studies are needed to unpick the relative role that young mosquitoes might have in disease transmission at the population level.

We show that mosquito abundance is significantly affected by the rate that fecundity declines with adult age. Despite the importance of age-dependent fecundity, there is a lack of data quantifying how the egg raft size changes at each gonotrophic cycle. This lack of data is driven by the experimental challenges of measuring egg raft size while controlling for the multitude of factors that affect mosquito egg-laying ability. The flexibility of our modelling approach allowed the theoretical exploration of the effects of age-dependent egg-laying, but it has highlighted a need for more detailed data on changes in egg raft size as *Cx. pipiens* age. Our modelling revealed that both larval abundances and the extent to which larval competition limits adult abundance can depend on how rapidly adult fecundity decreased with age.

We focused on the effects of temperature and age on adult mosquito abundance, without a detailed exploration of hydrological factors like humidity and variable rainfall. Humidity, an important abiotic factor expected to change in future decades (Byrne and Ogorman, 2016), is known to affect mosquito life history by influencing mosquito survival

and egg production (Brown et al., 2023). However, as noted by Brown et al. (2023), further research is needed to integrate humidity and its interaction with temperature into mechanistic models. Similarly, our model assumes a fixed habitat size, potentially overlooking variations in breeding site availability which, in turn, directly affects the strength of larval competition. Our assumption stems from the fact that incorporating larval habitat size into models is challenging due to limited knowledge about how factors such as breeding site availability, land use changes, and water management practices are likely to evolve under future climate scenarios (Shaman et al., 2010).

In summary, we have demonstrated that neglecting the age effect in mosquito mortality in modelling frameworks can potentially lead to underestimation of mosquito peak abundances. Our findings suggest that a steep decline in adult fecundity with age can increase or decrease adult abundance, depending on whether temperatures are warm enough to induce high levels of larval competition. By contrast, the decrease in adult abundance is not observed for these high temperatures when adult fecundity is age-independent. Therefore, we echo previous studies advocating that models aiming to capture mosquito population dynamics under climate change scenarios should incorporate senescence effects in their frameworks. Additionally, our model shows that when age effects are taken into account, increasing temperatures can have multiple effects on mosquito abundances, generally leading to increased adult peak abundances and to shifts in age distribution of the adult mosquito population towards an older age on average. Given that younger mosquitoes play a larger role in disease transmission and that increased mosquito abundances accentuate MBD outbreak risks, future climate scenarios are expected to affect MBD dynamics in multifaceted and opposing ways, which future research can help elucidate.

Declaration of competing interest

The authors declare that they have no conflict of interest.

CRediT authorship contribution statement

Renato Andrade: Writing – review & editing, Writing – original draft, Visualization, Validation, Software, Methodology, Investigation, Formal analysis, Conceptualization; **Steven M. White:** Writing – review & editing, Methodology, Investigation, Conceptualization; **Christina A. Cobbold:** Writing – review & editing, Writing – original draft, Supervision, Project administration, Methodology, Investigation, Formal analysis, Conceptualization

Acknowledgements

We thank Benedict Fellows and Dominic Brass for the insightful discussions during model conception stages. CAC and SMW were supported by the Engineering and Physical Sciences Research Council (EP/Y017919/1). SMW was supported by Mosquito Scotland UKRI-Defra BB/X018113/1.671.

Appendix A. Model details

A.1. Recruitment and survival expressions

The immature recruitment and maturation terms in Eq. (1) are given by

$$\begin{aligned} R_E(t) &= \frac{1}{2} \left[A_1(t)b_1(t) + \dots + A_N(t)b_N(t) + D_1(t)b_{D_1}(t) \right], \\ M_E(t) &= R_L(t) = R_E(t - \tau_E(t))S_E(t) \frac{g_E(t)}{g_E(t - \tau_E(t))}, \\ M_L(t) &= R_P(t) = R_L(t - \tau_L(t))S_L(t) \frac{g_L(t)}{g_L(t - \tau_L(t))}, \\ M_P(t) &= R_P(t - \tau_P(t))S_P(t) \frac{g_P(t)}{g_P(t - \tau_P(t))}, \end{aligned} \quad (15)$$

with $b_j(t)$ denoting the rate of egg-laying by adult females in class $A_j(t)$ per day, and $\tau_i(t)$, $g_i(t)$ are stage duration and development rates, respectively, of eggs ($i = E$), larvae ($i = L$) and pupae ($i = P$). The function $b_{D_1}(t)$ is the same as $b_1(t)$ with the difference that $b_{D_1}(t)$ is constrained to zero when photoperiod is decreasing ($\text{mod}(t, 365) < 173$, Forsythe et al., 1995), so that $D_1(t)$ adults only lays eggs after emerging from diapause. The stage durations $\tau_i(t)$ are determined by the equation

$$\frac{d\tau_i(t)}{dt} = 1 - \frac{g_i(t)}{g_i(t - \tau_i(t))}, \quad i = E, L, P, G. \quad (16)$$

In the case $i = G$, Eq. (16) describes the time evolution of the length of the gonotrophic cycle ($i = G$), $\tau_G(t)$.

The survival probability of stage i , S_i ($i = E, L, P$), is governed by equations

$$\begin{aligned} \frac{dS_E(t)}{dt} &= S_E(t) \left[\delta_E(t - \tau_E(t)) \frac{g_E(t)}{g_E(t - \tau_E(t))} - \delta_E(t) \right], \\ \frac{dS_L(t)}{dt} &= S_L(t) \left[\left(\delta_{DD}(L(t - \tau_L(t)), t - \tau_L(t)) + \delta_L(t - \tau_L(t)) \right) \frac{g_L(t)}{g_L(t - \tau_L(t))} \right. \\ &\quad \left. - \delta_L(t) - \delta_{DD}(L(t), t) \right], \\ \frac{dS_P(t)}{dt} &= S_P(t) \left[\delta_P(t - \tau_P(t)) \frac{g_P(t)}{g_P(t - \tau_P(t))} - \delta_P(t) \right]. \end{aligned} \quad (17)$$

A.2. Immature development and mortality

The functional forms for the development ($g_i(t)$) and mortality ($\delta_i(t)$) rates are fitted by Ewing et al. (2019) to experimental data available in the literature. The development rates are given by

$$g_i(t) = \begin{cases} \varphi_i T(t)^{\beta_i}, & \text{if } T(t) < \left(\frac{b_m}{\varphi_i}\right)^{\frac{1}{\beta_i}}, \quad (i \in \{E, L, P\}), \\ b_m, & \text{otherwise,} \end{cases} \quad (18)$$

and

$$g_G(t) = \frac{q_1}{1 + q_2 \exp(-q_3 T(t))}. \quad (19)$$

The mortality rates $\delta_i(t)$ are given by

$$\delta_i(t) = \max \left\{ v_{i0} \exp \left[\left(\frac{T(t) - v_{i1}}{v_{i2}} \right)^2 \right], b_m \right\} \quad i \in \{E, L, P\}, \quad (20)$$

where model parameters are given in Table A.8

A.3. Larval density-dependent mortality

The density-dependent larval mortality is given by

$$\delta_{DD}(L(t), t) = \delta_{LC}(L(t)) + \delta_\pi(L(t), t),$$

taken from Ewing et al. (2019), where

$$\delta_{LC}(L(t)) = c_0 \exp \left(\frac{c_1 L(t)}{V} \right), \quad (21)$$

describes larval intraspecific competition and

$$\delta_\pi(L(t), t) = \frac{a \mathcal{P}(t)}{V + ahL(t)}, \quad (22)$$

corresponds to larval predation, with predator density varying seasonally according to

$$\mathcal{P}(t) = r(t)L(t) = r_{\max} \left(\frac{1}{2} + \frac{1}{2} \sin \left(\frac{2\pi(t - v)}{365} \right) \right)^\chi L(t). \quad (23)$$

A.4. Rate of entering diapause

In this section we detail how we update the Ewing et al. (2019) model of diapause entry to track the age of mosquitoes entering diapause. We

begin by estimating the maximum rate at which adults enter diapause, Ψ (Eq. (6)). Estimating the rate of entering diapause is challenging, as the triggers for *Cx. pipiens* diapause are multiple (e.g., photoperiod, temperature, altitude, population genetics Field et al., 2022) and so using data from any experiment has limitations. We base our estimate on the data of Madder et al. (1983), which consists of daily egg-laying recordings for *Cx. pipiens* from May to September 1980. We use this data set as a proxy for adult activity since the dates for maximum and minimum egg-laying activity are consistent with the data from Ewing et al. (2019) on adult activity. The maximum egg-laying activity on 3rd of August ($t = 215$) is approximately 135 egg rafts. On the 30th of August ($t = 241$), 1 egg raft was observed, with egg-laying essentially stopping after August. Assuming that the number of eggs laid is proportional to the number of adults that are egg-laying and $A(t)$ is the adult population size at time t , we have

$$\frac{A(241)\zeta_{\text{aut}}(241)}{A(215)\zeta_{\text{aut}}(215)} = \frac{1}{135} \quad (24)$$

Ewing et al. (2019) assumed that the decrease in adult activity (measured by the number of adults collected in traps) in late summer was primarily due to adults entering diapause, rather than changes in adult abundance. Analogously, we assume that the change observed in the number egg rafts during August by Madder et al. (1983) was mostly due to adults entering diapause between $t = 215$ and $t = 241$ rather than changes in overall abundance. Hence, we have the relationship:

$$\dot{A}(t) = -A(t)\eta(t) \implies \log \left(\frac{A(241)}{A(215)} \right) = -\Psi \int_{215}^{241} (1 - \zeta_{\text{aut}}(t)) dt,$$

which leads to

$$\Psi = \frac{-\log \left(\frac{\zeta_{\text{aut}}(215)}{135\zeta_{\text{aut}}(241)} \right)}{\int_{215}^{241} (1 - \zeta_{\text{aut}}(t)) dt}. \quad (25)$$

By numerically integrating $1 - \zeta_{\text{aut}}(t)$ we obtain $\Psi \approx 0.1$.

A.5. Age-induced adult mortality

In this section we detail the model selection that led to the choice of function (Eq. (9)) used to describe how adult mortality increases with age. There are few experiments assessing age-dependent adult survival for multiple temperature values simultaneously for *Culex pipiens* (see however Papadopoulos et al., 2016), considering studies for other species of mosquitoes, we observe that the relationship between age and temperature on mortality can be complex (Brady et al., 2013; Miazgowicz et al., 2020). Given the lack of data, we assume that, other than the effect of temperature (T) on the length of the gonotrophic cycle ($\tau_G(T)$), the effect of age and temperature on adult mortality are independent and can be expressed as

$$\delta(T, t) = \underbrace{\mu_A(T)}_{\text{temperature}} \underbrace{f_{\tau_G}(t)}_{\text{age}}, \quad (26)$$

where $\mu_A(T)$ is the component of adult mortality purely dependent on temperature, parameterised by Ewing et al. (2016), assumed to be known, and $f_{\tau_G}(t)$ represents the age-dependent component of mortality. We assume that $f_{\tau_G}(t)$ is a step function in which all steps have length $\tau_G(T)$ and h_j is the value of $f_{\tau_G}(t)$ at the j th step. That is,

$$f_{\tau_G}(t) = h_j, \quad t \in [(j - 1)\tau_G(T), j\tau_G(T)), \quad \forall j \in \mathbb{N}^+. \quad (27)$$

Eq. (26) is fitted to data from Andreadis et al. (2014), which consists of survival curves for *Culex pipiens* adults under 5 different constant temperature scenarios: 15 °C, 20 °C, 25 °C, 27.5 °C, 30 °C. In the experiments, new-born adults (A_0) are monitored from $t = 0$. Hence, letting $A(t)$ represent the adult population at age t and $S_A(t)$ their survival, then

$$A(t) = A_0 S_A(t) \quad (28)$$

Table A.1
Model candidates and their corresponding AIC value.

Model name	h_j formula	Fit value	AIC value
Age-independent	1	-	269.0
Linear	κj	$\kappa = 0.395$	227.2
Quadratic	κj^2	$\kappa = 0.072$	210.6
Cubic	κj^3	$\kappa = 0.011$	205.6
Fourth order	κj^4	$\kappa = 0.002$	208.9
Gomperz/exponential	$\kappa_1 \exp(\kappa_2 j)$	$(\kappa_1, \kappa_2) = (0.120, 0.474)$	207.5

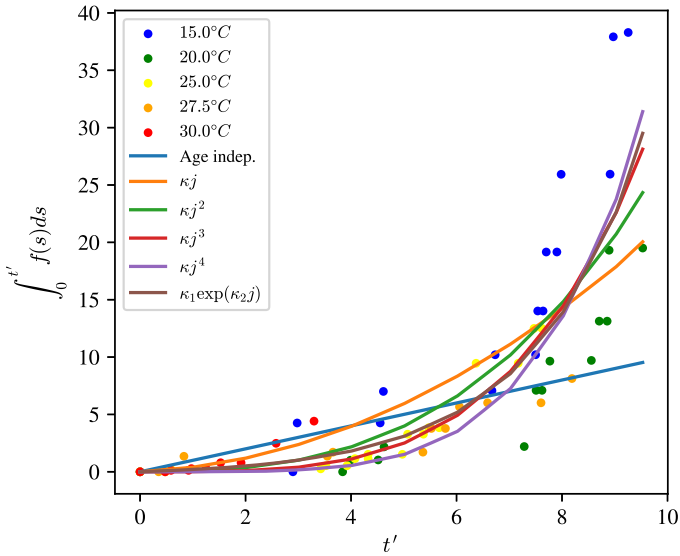


Fig. A.10. Comparison between the 5 models for age-dependent mortality (h_j), fitted to survival data from [Andreadis et al. \(2014\)](#), and an age-independent model. The age-independent model corresponds to $h_j = 1$.

and

$$S_A(t) = \exp \left[-\mu_A(T) \int_0^t f_{\tau_G}(s) ds \right]. \quad (29)$$

Hence,

$$\int_0^t f_{\tau_G}(s) ds = -\log(S_A(t))/\mu_A(T). \quad (30)$$

The data from [Andreadis et al. \(2014\)](#) corresponds to 5 different survival curves, one for each fixed temperature. We match each survival/temperature curve to $S_A(t)/T$ in our derivation. We use survival curves of the female adults.

In order to use the data for all temperatures simultaneously, we rescale time by the length of the gonotrophic cycle, setting $t' = t/\tau_G(T)$

in order to remove all the temperature dependency (through $\tau_G(T)$) from the left hand size of [Eq. \(30\)](#). This transformation corresponds to measuring time in terms of the number of gonotrophic cycles under constant temperature for all survival curves from [Andreadis et al. \(2014\)](#). We have that $f(s) = f_{\tau_G}(s\tau_G(T))$, where

$$f(s) = h_j, \quad \text{if } s \in [(j-1), j], \quad \forall j \in \mathbb{N}^+. \quad (31)$$

[Eq. \(30\)](#) then becomes

$$\int_0^{t'} f(s) ds = -\frac{\log(S_A(t'))}{\mu_A(T)\tau_G(T)}. \quad (32)$$

Therefore, by transforming the data of [Andreadis et al. \(2014\)](#) according to $t \rightarrow t/\tau_G(T) = t'$, $S_A(t) \rightarrow -\frac{\log(S_A(t'))}{\mu_A(T)\tau_G(T)}$, we are able to aggregate the survival curves $S_A(t')$ for the different temperatures and find the best fit for [Eq. \(32\)](#).

The models for h_j and their estimated AIC values are given in [Table A.1](#). The age-independent model ($h_j = 1, \forall j$) is included for completeness. The fitted curves for each model are shown in [Fig. A.10](#) and their corresponding residuals in [Fig. A.11](#).

The model with the lowest AIC value is the cubic model:

$$h_j = \kappa j^3 \quad (33)$$

with $\kappa = 0.01101 \pm 0.00057$.

The data from [Andreadis et al. \(2014\)](#) uses a relatively small number of mosquitoes (20 females for each temperature), which reduces the statistical power of our fitting. The limitation is particularly present at higher temperatures, in which mosquitoes often die at a very young age. This latter observation partially explains why the fitted model performs worse when compared to the 30 °C data ([Fig. A.12](#)), but otherwise performs well for lower temperatures. Moreover, most temperatures that we consider for North Kent Marshes in our simulations are below 30 °C.

A.6. Egg-laying

In [Fig. A.13](#) we show plots illustrating the shape of the function describing the relationship between adult fecundity and age (ρ_j , [Eq. \(12\)](#)), presented in [Section 2.3](#). All other results of the article are made using $\theta = 1.0$ ([Fig. A.13b](#)). Higher values of α correspond to a steeper decline in fecundity with adult age. In [Appendix B.2](#) we explore the effect of varying θ and α on the mosquito abundance profiles.

A.7. History function and inoculation

We assume that the system is empty before the start of the simulations ($t = t_0$). In other words:

$$E(t) = L(t) = P(t) = A_j(t) = D_j(t) = 0, \quad j \in \{1, 2, \dots, N\}, \forall t \leq t_0.$$

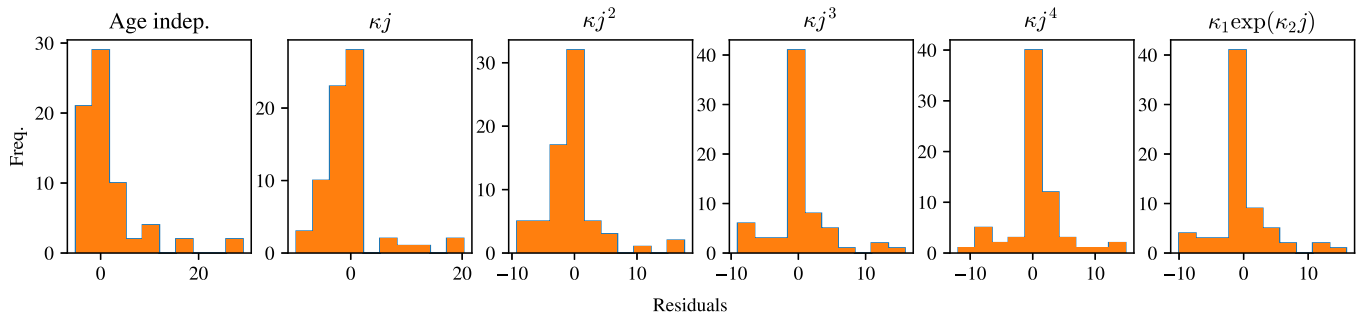


Fig. A.11. Residuals of fitting the models of age-dependent mortality given in [Table A.1](#).

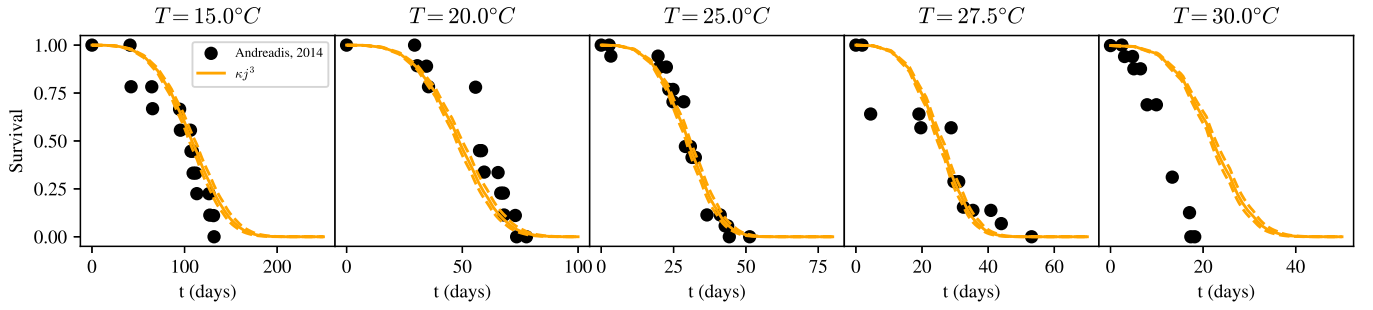


Fig. A.12. Selected model ($h_j = \kappa_j^3$) comparison to survival data recorded at different temperatures from Andreadis et al. (2014). Dashed lines: $\kappa = 0.01101 \pm 2$ standard deviations curves.

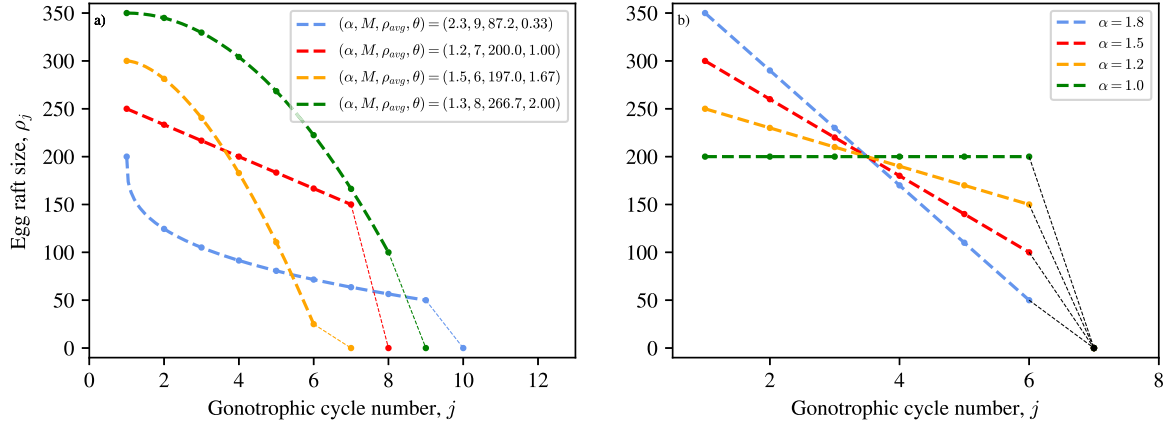


Fig. A.13. Plots of egg raft size (ρ_j) as functions of gonotrophic cycle number (j) determined by Eq. (12). (a) curves for different values of α , ρ_{avg} , M and θ . (b) $\theta = 1.0$, $M = 6$ and average raft size is 200 for all curves. We refer to the $\alpha = 1$ case as the age-independent fecundity case.

The history functions for $S_i(t)$, $\tau_i(t)$ follow Ewing et al. (2019), and are given by

$$\tau_i(t) = \frac{1}{g_i(t)}, \quad i \in \{E, L, P, G\}$$

and

$$S_i(t) = \exp\left(-\frac{\delta_i(t)}{g_i(t)}\right), \quad i \in \{E, L, P\},$$

for all $t \leq t_0$. Similarly, for the adult survival

$$S_{A_j}(t) = \exp\left(-\frac{\delta_{A_j}(t)}{g_G(t)}\right), \quad j \in \{1, 2, \dots, N\}, \quad \forall t \leq t_0.$$

Adult individuals are inoculated into the $A_1(t)$ class at time $t = t_0$ according to the following function

$$I(t) = \begin{cases} J_0/\Delta t, & \text{if } t_0 < t \leq t_0 + \Delta t, \\ 0, & \text{otherwise,} \end{cases} \quad (34)$$

where $I(t)$ represents the rate at which $A_1(t)$ adults are being inoculated into the system and J_0 is the number of adult mosquitoes inoculated.

A.8. Table of model parameters

Table A.2 lists the set of parameters taken from Ewing et al. (2019). The additional parameters introduced in our model are given in Table A.3. Values for Ψ and κ were determined based on the empirical data of Madder et al. (1983) and Andreadis et al. (2014), as discussed in Section A.4 and Section A.5, respectively.

Table A.2

Parameter values taken from Ewing et al. (2019).

Parameter	Definition	Value
φ_E	Fit parameter in egg maturation ($\text{days}^{-1} \circ \text{C}^{-\beta_E}$)	2.20×10^{-3}
β_E	Fit parameter in egg maturation	1.77
φ_L	Fit parameter in larval maturation ($\text{days}^{-1} \circ \text{C}^{-\beta_L}$)	3.15×10^{-3}
β_L	Fit parameter in larval maturation	1.12
φ_P	Fit parameter in pupal maturation ($\text{days}^{-1} \circ \text{C}^{-\beta_P}$)	7.11×10^{-4}
β_P	Fit parameter in pupal maturation	1.89
$\mu_{0E}, \mu_{0L}, \mu_{0P}$	Baseline immature mortality rate (days^{-1})	0.0157
$\mu_{1E}, \mu_{1L}, \mu_{1P}$	Optimum temperature for immature survival ($^\circ\text{C}$)	20.5
$\mu_{2E}, \mu_{2L}, \mu_{2P}$	Width parameter for immature death rate ($^\circ\text{C}$)	7
φ_A	Fit parameter for adult mortality ($\text{days}^{-1} \circ \text{C}^{-\beta_A}$)	2.17×10^{-8}
β_A	Fit parameter for adult mortality	4.48
b_m	Baseline maturation (egg, larval, pupal) (days^{-1})	$\frac{1}{60}$
b_{di}	Threshold immature mortality rate (days^{-1})	1
b_{da}	Baseline diapausing adults mortality rate (days^{-1})	0.006
c_0	Fit parameter in competition (days^{-1})	0.00319
c_1	Fit parameter in competition (L larvae $^{-1}$)	0.00469
a	Attack rate of predators (predator $^{-1}$ days $^{-1}$)	1.03
h	Handling time (predator L larvae $^{-1}$ days $^{-1}$)	0.0043
r_{\max}	Peak predator per larvae (predator L larvae $^{-1}$)	0.0214
v	Predation time parameter (days^{-1})	19.84
χ	Predation sharpness parameter	2.45
V	Volume of larval habitat (L)	20
q_1	Gonotrophic cycle fit parameter (days^{-1})	0.202
q_2	Gonotrophic cycle fit parameter	74.5
q_3	Gonotrophic cycle fit parameter ($^\circ\text{C}^{-1}$)	0.246
ξ_{spr}	Spring diapause threshold (hours)	13.7
ξ_{aut}	Autumn diapause threshold (hours)	15
ω_{spr}	Spring diapause transition sensitivity	5
ω_{aut}	Autumn diapause transition sensitivity	3.5
Γ	Post-diapause mortality parameter	10
σ^2	Post-diapause mortality duration 2 (days^2)	4
D	Diapause exit threshold day of the year	109
\mathcal{L}	Latitude used in the model for the photoperiod	51.6
\mathcal{S}	Sunset parameter used in the photoperiod model	0.8333

Table A.3
Additional parameters introduced in the age-dependent model.

Parameter	Definition	Value
Ψ	Maximum rate of entering diapause (days^{-1})	0.1
κ	Fit parameter in age-dependent mortality	0.0110
θ	Curvature in age-dependent fecundity	1.0
N	Number of adult age classes	10
M	Number of adult age classes that lay eggs	6

Appendix B. Supplementary results

B.1. Varying the number of egg-laying adult classes

In our model, we consider $N = 10$ adult age classes. Adults in age classes 1 to M lay eggs. In Fig. B.14 we illustrate the effect of varying the number of adult classes that lay eggs (M). For $M > 6$, adult abundances at the diapausing and summer peaks are not changed by further increases of M . The contribution to population abundance of egg-laying adults that reach adult class beyond the 6th is negligible because a 6th gonotrophic cycle is only reached late in the season, when adults are already entering diapause.

B.2. Comparison between the effect of θ and α

In this section we explore how the shape of the relationship between fecundity and age affects adults abundance. We vary the curvature (θ) of the function and how strongly fecundity declines with age (α). In Fig. B.15, heatmaps illustrate adult abundances at the summer peak and the diapause peak for multiple values of (θ, α) . Two temperature scenarios are considered. For temperature values corresponding to the recorded temperature from 1960 to 90 (Fig. B.15a, c), the parameter θ has little effect on peak size, both for the summer and diapause peaks (no more than a 6% change in peak size by varying the value of θ alone). For RCP 4.5 2080 temperature projections, the value of θ has little effect on abundance in comparison to the effect of changing α (Fig. B.15b, d).

For example, at large values of α , the diapausing peak (Fig. B.15d) does not change size by more than 3% as θ is varied.

B.3. Increased fecundity of younger adults

B.4. Adult age composition

In this section we explore how temperature and the rate that fecundity declines with age (α) affect the adult age distribution. We consider how the proportion of adults in each age class changes over time (Fig. B.16) and focus our discussion on the contribution of the young adults, $A_1(t)$, to the total egg-laying adult population over the full egg-laying period. Overall, we observe that in all plots, the younger adults compose the majority of the adult population early in the season. In late summer and early autumn, the adult population is composed mostly of older individuals. Moreover, our simulations show that increasing α alone does not significantly increase the total percentage of $A_1(t)$ over the entire course of the egg-laying season. This is illustrated both for the 1960–60 historical record case (Fig. B.16a–c) and the RCP 4.5 2050s temperature projection case (Fig. B.16d–f) scenarios. In each of the two temperature scenarios, the percentage of young adults does not change by more than 2% by varying α alone. However, for fixed α , if we compare the percentage of $A_1(t)$ adults under 1960–90 temperatures to those under RCP 4.5 2050 projections (e.g., comparing Fig. B.16a to d), we observe a noticeable decrease in the percentage of $A_1(t)$ for each value of α . The decrease in the percentage of $A_1(t)$ adults as temperature increased is due to the warmer summer temperatures (increased μ and λ), which decrease the length of the gonotrophic cycle and more adults reach the older classes before the summer is over. Therefore, under increased temperatures, the age composition of the active adult population shifts towards older adults, as indicated by the orange and red plots in Fig. B.16d–f. A similar shift in the age composition of the adult population towards older adult classes is obtained when increasing the length of the summer (not shown).

B.5. Larval density-dependent mortality

Here we illustrate that presence of high larval competition when both temperature is high and fecundity declines rapidly with age (high α). Fig. B.17 shows the larval mortality rate due density-dependent competition (Eq. (21)) for two different temperature regimes: 1960–90

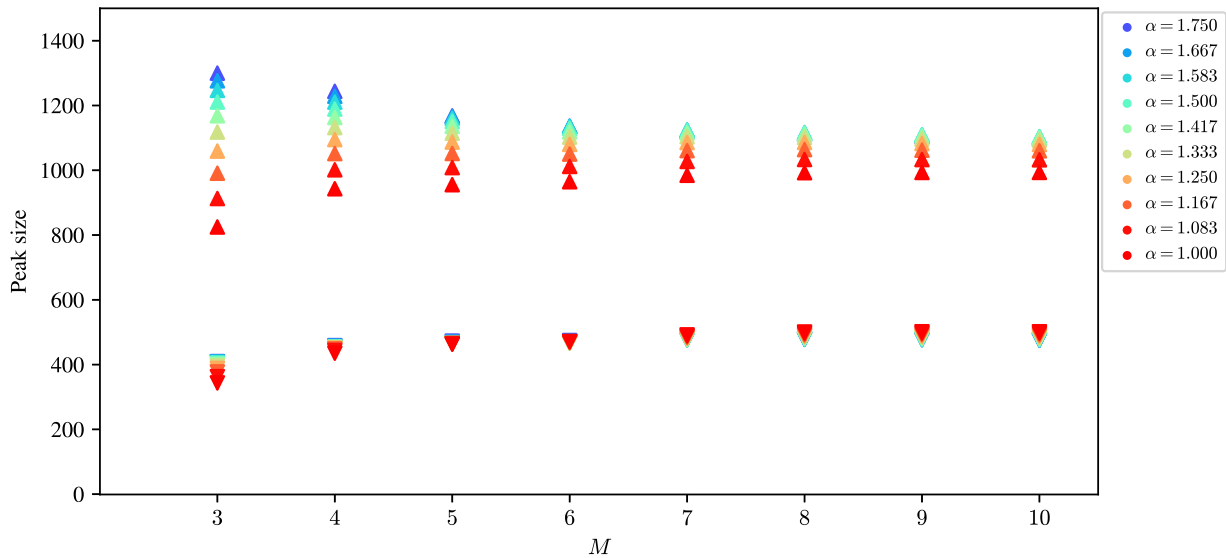


Fig. B.14. The size of adult summer peaks (Δ) and diapause peaks (∇) in the last year of a 7 year simulation, for different values of α and M . Upward triangles: summer peaks. Downward triangles: diapause peaks. Temperature parameters are $(\mu, \lambda, \phi, \gamma) = (10.80, 6.38, 0.55, 1.25)$ which correspond to 1960–90 temperature values (Hollis, 2017).

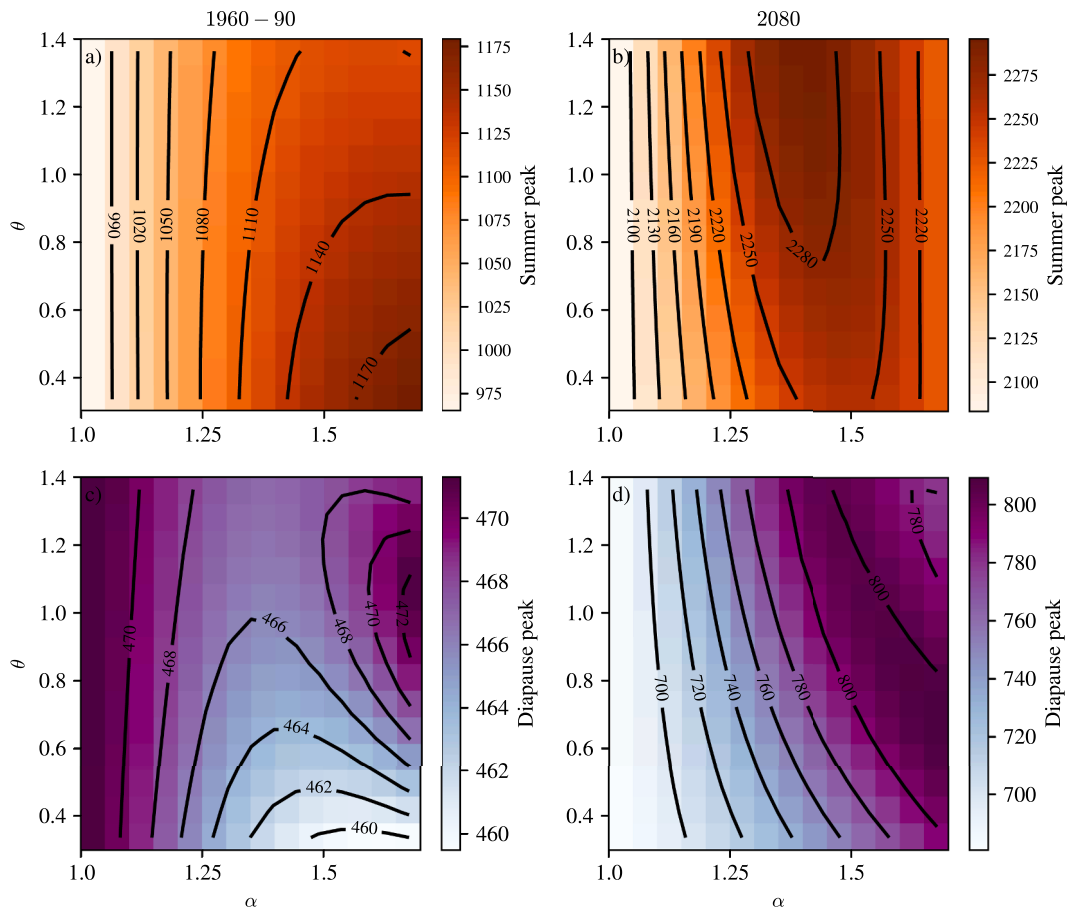


Fig. B.15. Heatmaps for adult summer and diapausing peaks during the final year of a 7 year simulation for different values of adult fecundity parameters, θ (curvature) and α (the rate at which fecundity declines with age). When $\alpha = 1.0$, adult fecundity is age-independent. Temperature scenarios are (a,c) 1960–1990 historical records (Hollis, 2017) and (b,d) RCP 4.5 projections for 2080s (Met Office Hadley Centre, 2018).

temperatures, in blue and RCP 4.5 2080s projections in red, for multiple values of α . As a reference for comparison, we also plot larval mortality rate due predation (Eq. (22)). The blue curves show a smaller contribution from competition (continuous lines) to larval mortality compared to predation (dashed lines), for all values of α . When temperatures are increased to RCP 4.5 2080s projections (red), the larval population has increased sufficiently that larval competition is high, whereas levels of larval predation remain almost unchanged. Moreover, in each temperature scenario, by comparing the more transparent curves to the more opaque curves, the effect of competition is increased as we increase the rate that adult fecundity declines with age (increasing α). Therefore, under the high temperature scenario (RCP 4.5 2080s), despite the large larval population, the increased competition results in fewer individuals reaching adulthood when compared to the 1960–90 temperature scenario. Increased competition-induced larval mortality is the mechanism behind the decrease in adult summer peak abundances found when both temperature and α are high (Figs. 5c, 7b, 8c).

B.6. Timing of the peak

In this section we illustrate how the age structure of the population affects the timing of the adult summer peaks. When adult fecundity declines more rapidly with age (increasing α), larval and adult stages peak in abundance earlier in the year, in all temperature scenarios (Fig. 7a). The peak abundances happen earlier as we increase α due to a relative increase in egg-laying by young adults, which are present earlier in the year, as discussed in Section 3.3. Moreover, increasing temperature (denoted by moving from blue to red markers) causes the peaks to shift even earlier. This is due each temperature scenario (RCP 4.5 2020s, 2050s, 2080s) having progressively larger mean temperatures values (larger μ 's), resulting in higher temperatures in spring. Hence, immature development time and gonotrophic cycle length tend to be smaller in spring, causing the population peaks to occur earlier in the year as we move from RCP 4.5 2020s towards RCP 4.5 2080s.

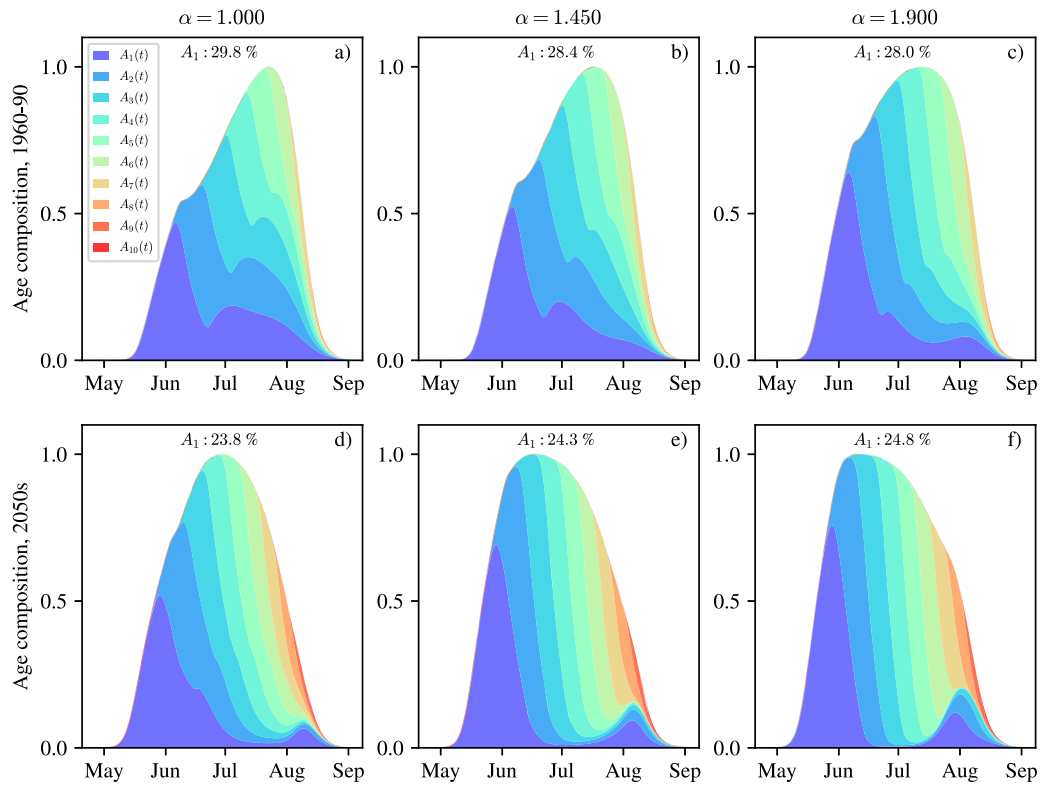


Fig. B.16. Stack plot of the age composition of the egg-laying active adults ($\zeta(t)A_j(t)$, $j = 1, 2, \dots, M$) for the (a–c) 1960–90 historical records and the (d–f) RCP 4.5 - 2050s temperature projections, for three values values of α (the rate at which fecundity declines with age). Plots are of normalised abundances over the last year of 7 year simulations. The percentages correspond to contribution of the first adult class ($A_1(t)$) to the population, considered over the entire egg-laying period.

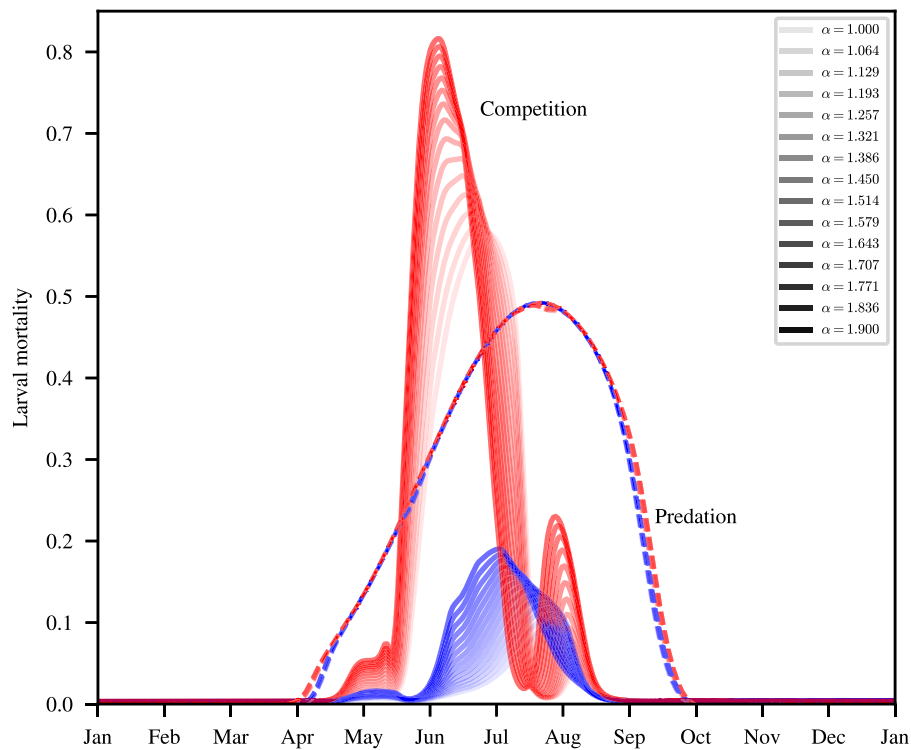


Fig. B.17. Components of density dependent larval mortality in days^{-1} , for 1960–90 (blue) and RCP 4.5 - 2080s (red) temperatures. Continuous lines denote the amount of mortality due to larval competition, dashed lines correspond to the effect of predation component of larval mortality. The transparency of the curves correspond to different values of α , with opaque curves corresponding to the highest declines of fecundity with adult age.

Timing of the larvae and adult summer peaks

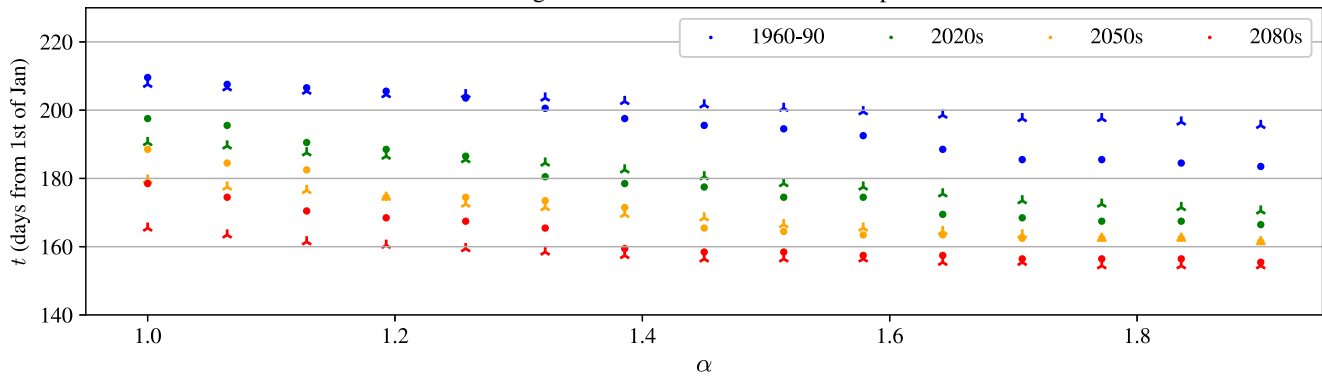


Fig. B.18. Timing of the summer larval (circles) and adult (three-pointed stars) peaks as a function of α for temperatures corresponding to 1960–90 daily temperatures (blue), RCP 4.5 - 2020s (green), RCP 4.5 - 2050s (orange) and RCP 4.5 - 2080s (red) maximum probability projections.

References

- Agnew, P., Haussy, C., Michalakakis, Y., 2000. Effects of density and larval competition on selected life history traits of *Culex pipiens quinquefasciatus* (Diptera: Culicidae). *J. Med. Entomol.* 37 (5), 732–735.
- Akoh, J.I., Aigbodion, F.I., Kumbak, D., 1992. Studies on the effect of larval diet, adult body weight, size of blood-meal and age on the fecundity of *Culex quinquefasciatus* (Diptera: Culicidae). *Int. J. Trop. Insect Sci.* 13 (2), 177–181.
- Amarasekare, P., Coutinho, R.M., 2014. Effects of temperature on intraspecific competition in ectotherms. *Am. Nat.* 184 (3), E50–E65.
- Andrade, R., White, S., Cobbold, C., 2025. MosquitoAge-DDE v1.0. <https://doi.org/10.5525/gla.researchdata.1861>.
- Andreadis, S.S., Dimotisiou, O.C., Savopoulou-Soultani, M., 2014. Variation in adult longevity of *Culex pipiens f. pipiens*, vector of the West Nile virus. *Parasitol. Res.* 113, 4315–4319.
- Awahmukalah, D. S.T., Brooks, M.A., 1985. Viability of *Culex pipiens pipiens* eggs affected by nutrition and aposymbiosis. *J. Invertebr. Pathol.* 45 (2), 225–230.
- Bailey, C.L., Faran, M.E., Gargan, I.L., Thomas, P., Hayes, D.E., 1982. Winter survival of blood-fed and nonblood-fed *Culex pipiens* L. Technical Report. Army Medical Research Institute of Infectious Diseases Fort Detrick, MD.
- Bakran-Lebl, K., Kjær, L.J., Conrady, B., 2023. Predicting *Culex pipiens/restuans* population dynamics using a weather-driven dynamic compartmental population model. *Insects* 14 (3), 293.
- Barker, C.M., Eldridge, B.F., Reisen, W.K., 2010. Seasonal abundance of *Culex tarsalis* and *Culex pipiens* complex mosquitoes (Diptera: Culicidae) in California. *J. Med. Entomol.* 47 (5), 759–768.
- Bellan, S.E., 2010. The importance of age dependent mortality and the extrinsic incubation period in models of mosquito-borne disease transmission and control. *PLoS One* 5 (4), e10165.
- Brady, O.J., Johansson, M.A., Guerra, C.A., Bhatt, S., Golding, N., Pigott, D.M., Delatte, H., Grech, M.G., Leishman, P.T., Maciel-de Freitas, R., et al., 2013. Modelling adult *Aedes aegypti* and *Aedes albopictus* survival at different temperatures in laboratory and field settings. *Parasit. Vectors* 6 (1), 1–12.
- Brass, D.P., Cobbold, C.A., Purse, B.V., Ewing, D.A., Callaghan, A., White, S.M., 2024. Role of vector phenotypic plasticity in disease transmission as illustrated by the spread of dengue virus by *Aedes albopictus*. *Nat. Commun.* 15 (1), 7823.
- Brown, J.J., Pascual, M., Wimberly, M.C., Johnson, L.R., Murdock, C.C., 2023. Humidity—the overlooked variable in the thermal biology of mosquito-borne disease. *Ecol. Lett.* 26 (7), 1029–1049.
- Brugman, V.A., Hernández-Triana, L.M., Medlock, J.M., Fooks, A.R., Carpenter, S., Johnson, N., 2018. The role of *Culex pipiens* L. (Diptera: Culicidae) in virus transmission in Europe. *Int. J. Environ. Res. Public Health* 15 (2), 389.
- Byrne, M.P., Ogorman, P.A., 2016. Understanding decreases in land relative humidity with global warming: conceptual model and GCM simulations. *J. Clim.* 29 (24), 9045–9061.
- Cailly, P., Tran, A., Balenghien, T., Lambert, G., Toty, C., Ezanno, P., 2012. A climate-driven abundance model to assess mosquito control strategies. *Ecol. Model.* 227, 7–17.
- Caldwell, J.M., LaBeaud, A.D., Lambin, E.F., Stewart-Ibarra, A.M., Ndenga, B.A., Mutuku, F.M., Krystosik, A.R., Ayala, E.B., Anyamba, A., Borbor-Cordova, M.J., et al., 2021. Climate predicts geographic and temporal variation in mosquito-borne disease dynamics on two continents. *Nat. Commun.* 12 (1), 1233.
- Caminade, C., McIntyre, K.M., Jones, A.E., 2019. Impact of recent and future climate change on vector-borne diseases. *Ann. N. Y. Acad. Sci.* 1436 (1), 157–173.
- Chala, B., Hamde, F., 2021. Emerging and re-emerging vector-borne infectious diseases and the challenges for control: a review. *Front. Public Health* 9, 715759.
- Ciota, A.T., Maccachiero, A.C., Kilpatrick, A.M., Kramer, L.D., 2014. The effect of temperature on life history traits of *Culex* mosquitoes. *J. Med. Entomol.* 51 (1), 55–62.
- Clements, A.N., Paterson, G.D., 1981. The analysis of mortality and survival rates in wild populations of mosquitoes. *J. Appl. Ecol.* 18, 373–399.
- Davis, E.L., Hollingsworth, T.D., Keeling, M.J., 2024. An analytically tractable, age-structured model of the impact of vector control on mosquito-transmitted infections. *PLoS Comput. Biol.* 20 (3), e1011440.
- Delatte, H., Gimonneau, G., Triboire, A., Fontenille, D., 2009. Influence of temperature on immature development, survival, longevity, fecundity, and gonotrophic cycles of *Aedes albopictus*, vector of chikungunya and dengue in the Indian ocean. *J. Med. Entomol.* 46 (1), 33–41.
- Deutsch, C.A., Tewksbury, J.J., Huey, R.B., Sheldon, K.S., Ghalambor, C.K., Haak, D.C., Martin, P.R., 2008. Impacts of climate warming on terrestrial ectotherms across latitude. *Proc. Natl. Acad. Sci.* 105 (18), 6668–6672.
- Diaz-Badillo, A., Bolling, B.G., Perez-Ramirez, G., Moore, C.G., Martinez-Munoz, J.P., Padilla-Viveros, A.A., Camacho-Nuez, M., Diaz-Perez, A., Beaty, B.J., de Lourdes Munoz, M., 2011. The distribution of potential West Nile virus vectors, *Culex pipiens pipiens* and *Culex pipiens quinquefasciatus* (Diptera: Culicidae), in Mexico City. *Parasit. Vectors* 4 (1), 1–12.
- Driver, R.D., 2012. Ordinary and Delay Differential Equations. Springer New York, NY.
- El-Sayed, A., Kamel, M., 2020. Climatic changes and their role in emergence and re-emergence of diseases. *Environ. Sci. Pollut. Res.* 27, 22336–22352.
- Ewing, D.A., 2017. Modelling the phenological effects of environmental drivers on mosquito abundance: implications for West Nile Virus transmission potential in the UK. Ph.D. thesis. University of Glasgow.
- Ewing, D.A., Cobbold, C.A., Purse, B.V., Nunn, M.A., White, S.M., 2016. Modelling the effect of temperature on the seasonal population dynamics of temperate mosquitoes. *J. Theor. Biol.* 400, 65–79.
- Ewing, D.A., Purse, B.V., Cobbold, C.A., Schäfer, S.M., White, S.M., 2019. Uncovering mechanisms behind mosquito seasonality by integrating mathematical models and daily empirical population data: *Culex pipiens* in the UK. *Parasit. Vectors* 12 (1), 1–19.
- Farajollahi, A., 2005. Seasonal dynamics of *Culex pipiens pipiens* L. (Diptera: Culicidae) in New Jersey and examination of its role as an overwintering reservoir for West Nile Virus. Ph.D. thesis. Rutgers University.
- Field, E.N., Shepard, J.J., Clifton, M.E., Price, K.J., Witmier, B.J., Johnson, K., Boze, B., Abadam, C., Ebel, G.D., Armstrong, P.M., et al., 2022. Semi-field and surveillance data define the natural diapause timeline for *Culex pipiens* across the United States. *Commun. Biol.* 5 (1), 1300.
- Forsythe, W.C., Rykiel, E.J., Jr, Stahl, R.S., Wu, H.-i., Schoolfield, R.M., 1995. A model comparison for daylength as a function of latitude and day of year. *Ecol. Model.* 80 (1), 87–95.
- Franklins, L. H.V., Jones, K.E., Redding, D.W., Abubakar, I., 2019. The effect of global change on mosquito-borne disease. *Lancet Infect. Dis.* 19 (9), e302–e312.
- Frantz, R.M., Godinez, H., Martinez, K., Cuellar, W.S., Manore, C., 2024. Age structured partial differential equations model for *Culex* mosquito abundance. *Ecol. Model.* 494, 110764. <https://www.sciencedirect.com/science/article/pii/S0304388024001522>. <https://doi.org/10.1016/j.ecolmodel.2024.110764>
- Gangoso, L., Aragonés, D., Martínez-de la Puente, J., Lucientes, J., Delacour-Estrella, S., Peña, R.E., Montalvo, T., Bueno-Marí, R., Bravo-Barriga, D., Frontera, E., et al., 2020. Determinants of the current and future distribution of the West Nile virus mosquito vector *Culex pipiens* in Spain. *Environ. Res.* 188, 109837.
- Golding, N., Nunn, M.A., Medlock, J.M., Purse, B.V., Vaux, A. G.C., Schäfer, S.M., 2012. West Nile virus vector *Culex modestus* established in Southern England. *Parasit. Vectors* 5, 1–5.
- Gratz, N.G., 1999. Emerging and resurging vector-borne diseases. *Annu. Rev. Entomol.* 44 (1), 51–75.
- Hahn, D.A., Denlinger, D.L., 2007. Meeting the energetic demands of insect diapause: nutrient storage and utilization. *J. Insect Physiol.* 53 (8), 760–773.
- Hardy, J.L., Houk, E.J., Kramer, L.D., Reeves, W.C., 1983. Intrinsic factors affecting vector competence of mosquitoes for arboviruses. *Annu. Rev. Entomol.* 28 (1), 229–262.
- Harrington, L.C., Françoisvermeulen, n., Jones, J.J., Kithawee, S., Sithiprasasna, R., Edman, J.D., Scott, T.W., 2014. Age-dependent survival of the dengue vector *Aedes aegypti* (Diptera: Culicidae) demonstrated by simultaneous release–recapture of different age cohorts. *J. Med. Entomol.* 45 (2), 307–313.
- Hollis, M., 2017. UKCP09: Met-office gridded and regional land surface climate observation datasets. Centre for environmental data analysis <http://catalogue.ceda.ac.uk/uuid/87f43af9d0e242f483351d79b3d6162a> (accessed on August 2023).

- Hongoh, V., Berrang-Ford, L., Scott, M.E., Lindsay, L.R., 2012. Expanding geographical distribution of the mosquito, *Culex pipiens*, in Canada under climate change. *Appl. Geogr.* 33, 53–62.
- Jaenson, T. G.T., 1987. Overwintering of *Culex* mosquitoes in Sweden and their potential as reservoirs of human pathogens. *Med. Vet. Entomol.* 1 (2), 151–156.
- Johnson, B.J., Hugo, L.E., Churcher, T.S., Ong, O. T.W., Devine, G.J., 2020. Mosquito age grading and vector-control programmes. *Trends Parasitol.* 36 (1), 39–51.
- Kamgang, J.C., Kamla, V.C., Tchoumi, S.Y., et al., 2014. Modeling the dynamics of malaria transmission with bed net protection perspective. *Appl. Math.* 5 (19), 3156.
- Kershaw, W.E., Chalmers, T.A., Lavoipierre, M., 1954. Studies on arthropod survival: I.—The pattern of mosquito survival in laboratory conditions. *Ann. Trop. Med. Parasitol.* 48 (4), 442–450.
- Knecht, H., Richards, S.L., Balanay, J. A.G., White, A.V., 2018. Impact of mosquito age and insecticide exposure on susceptibility of *Aedes albopictus* (Diptera: Culicidae) to infection with Zika virus. *Pathogens* 7 (3), 67.
- Koenraad, C. J.M., Möhlmann, T. W.R., Verhulst, N.O., Spitzen, J., Vogels, C. B.F., 2019. Effect of overwintering on survival and vector competence of the West Nile virus vector *Culex pipiens*. *Parasit. Vectors* 12 (1), 1–9.
- Liu, B., Gao, X., Zheng, K., Ma, J., Jiao, Z., Xiao, J., Wang, H., 2020. The potential distribution and dynamics of important vectors *Culex pipiens pallens* and *Culex pipiens quinquefasciatus* in China under climate change scenarios: an ecological niche modelling approach. *Pest Manag. Sci.* 76 (9), 3096–3107.
- Liu, L., Zhang, B., Cheng, P., Wang, H., Guo, X., Zhang, C., Wang, H., Zhao, Y., Gong, M., 2016. Overwintering of *Culex pipiens pallens* (Diptera: Culicidae) in Shandong, China. *J. Entomol. Sci.* 51 (4), 314–320.
- Loetti, V., Schweigmann, N., Burrioni, N., 2011. Development rates, larval survivorship and wing length of *Culex pipiens* (Diptera: Culicidae) at constant temperatures. *J. Nat. Hist.* 45 (35–36), 2203–2213.
- Lončarić, Ž., Hackenberger, B.K., 2013. Stage and age structured *Aedes vexans* and *Culex pipiens* (Diptera: Culicidae) climate-dependent matrix population model. *Theor. Popul. Biol.* 83, 82–94.
- Madder, D.J., Surgeoner, G.A., Helson, B.V., 1983. Number of generations, egg production, and developmental time of *Culex pipiens* and *Culex restuans* (Diptera: Culicidae) in southern Ontario. *J. Med. Entomol.* 20 (3), 275–287.
- Makiya, K., Sakurai, H., 1975. Survival of the overwintering house mosquito, *Culex pipiens pallens*, with special reference to the relation between wing length and survival rate. *Med. Entomol. Zool.* 26 (1), 7–14.
- Manguin, S., Boëte, C., 2011. The Importance of Biological Interactions in the Study of Biodiversity. *Tech. Rijeka Croatia*. chapter 3. pp. 27–50.
- Mayton, E.H., Tramonte, A.R., Wearing, H.J., Christofferson, R.C., 2020. Age-structured vectorial capacity reveals timing, not magnitude of within-mosquito dynamics is critical for arbovirus fitness assessment. *Parasit. Vectors* 13, 1–13.
- McCann, S., Day, J.F., Allan, S., Lord, C.C., 2009. Age modifies the effect of body size on fecundity in *Culex quinquefasciatus* Say (Diptera: Culicidae). *J. Vector Ecol.* 34 (2), 174–181.
- Met Office Hadley Centre, 2018. UKCP18 regional climate model projections for the UK. Centre for environmental data analysis <https://ukclimateprojections-uk.metoffice.gov.uk/ui/home> (accessed on August 2023).
- Metelmann, S., Caminade, C., Jones, A.E., Medlock, J.M., Baylis, M., Morse, A.P., 2019. The UKs suitability for *Aedes albopictus* in current and future climates. *J. R. Soc. Interface* 16 (152), 20180761.
- Miazgowicz, K.L., Shocket, M.S., Ryan, S.J., Villena, O.C., Hall, R.J., Owen, J., Adanlawo, T., Balaji, K., Johnson, L.R., Mordecai, E.A., et al., 2020. Age influences the thermal suitability of *Plasmodium falciparum* transmission in the Asian malaria vector *Anopheles stephensi*. *Proc. R. Soc. B* 287 (1931), 20201093.
- Mitchell, C.J., Briegel, H., 1989. Inability of diapausing *Culex pipiens* (Diptera: Culicidae) to use blood for producing lipid reserves for overwinter survival. *J. Med. Entomol.* 26 (4), 318–326.
- Mohammed, A., Chadee, D.D., 2011. Effects of different temperature regimens on the development of *Aedes aegypti* (L.) (Diptera: Culicidae) mosquitoes. *Acta Trop.* 119 (1), 38–43.
- Mordecai, E.A., Caldwell, J.M., Grossman, M.K., Lippi, C.A., Johnson, L.R., Neira, M., Rohr, J.R., Ryan, S.J., Savage, V., Shocket, M.S., et al., 2019. Thermal biology of mosquito-borne disease. *Ecol. Lett.* 22 (10), 1690–1708.
- Nelms, B.M., Macedo, P.A., Kothera, L., Savage, H.M., Reisen, W.K., 2013. Overwintering biology of *Culex* (Diptera: Culicidae) mosquitoes in the Sacramento Valley of California. *J. Med. Entomol.* 50 (4), 773–790.
- Nielsen, S.S., Alvarez, J., Bicut, D.J., Calistri, P., Depner, K., Drewe, J.A., Garin-Bastuji, B., Rojas, J. L.G., Schmidt, C.G., Michel, V., et al., 2020. Rift valley fever—epidemiological update and risk of introduction into Europe. *EFSA J.* 18 (3), e06041.
- Nisbet, R.M., Gurney, W., 1983. The systematic formulation of population models for insects with dynamically varying instar duration. *Theor. Popul. Biol.* 23 (1), 114–135.
- Organization, W.H., 2022. Vector-borne diseases <https://www.who.int/en/news-room/fact-sheets/detail/vector-borne-diseases>.
- Papadopoulos, N.T., Carey, J.R., Ioannou, C.S., Ji, H., Mueller, H.-G., Wang, J.-L., Luckhart, S., Lewis, E.E., 2016. Seasonality of post-capture longevity in a medically important mosquito (*Culex pipiens*). *Front. Ecol. Evol.* 4, 63.
- Pigeault, R., Nicot, A., Gandon, S., Rivero, A., 2015. Mosquito age and avian malaria infection. *Malar. J.* 14, 1–11.
- Ramzy, R. M.R., Kamal, H.A., Hassan, M.A., Haggag, A.A., 2019. Elimination of lymphatic filariasis as a public health problem from the Arab Republic of Egypt. *Acta Trop.* 199, 105121.
- Richards, S.L., Lord, C.C., Pesko, K., Tabachnick, W.J., 2009. Environmental and biological factors influencing *Culex pipiens quinquefasciatus* Say (Diptera: Culicidae) vector competence for Saint Louis encephalitis virus. *Am. J. Trop. Med. Hyg.* 81 (2), 264.
- Rock, K.S., Wood, D.A., Keeling, M.J., 2015. Age-and bite-structured models for vector-borne diseases. *Epidemics* 12, 20–29.
- Rogers, D.J., Randolph, S.E., 2006. Climate change and vector-borne diseases. *Adv. Parasitol.* 62, 345–381.
- Roubaud, E., 1944. Sur la fécondité du moustique commun, *Culex pipiens* L. *Bull. Soc. Pathol. Exot.* 37 (1–2), 51–56.
- Samarawickrema, W.A., 1967. A study of the age-composition of natural populations of *Culex pipiens fatigans* Wiedemann in relation to the transmission of filariasis due to *Wuchereria bancrofti* (Cobbold) in Ceylon. *Bull. World Health Organ.* 37 (1), 117.
- Semenza, J.C., Suk, J.E., 2018. Vector-borne diseases and climate change: a European perspective. *FEMS Microbiol. Lett.* 365 (2), fnx244.
- Shaman, J., Day, J.F., Komar, N., 2010. Hydrologic conditions describe West Nile virus risk in Colorado. *Int. J. Environ. Res. Public Health* 7 (2), 494–508.
- Shelton, R.M., et al., 1973. The effect of temperatures on development of eight mosquito species. *Mosq. News* 33 (1), 1–12.
- Siria, D.J., Sanou, R., Mitton, J., Mwanga, E.P., Niang, A., Sare, I., Johnson, P. C.D., Foster, G.M., Belem, A. M.G., Wynne, K., et al., 2022. Rapid age-grading and species identification of natural mosquitoes for malaria surveillance. *Nat. Commun.* 13 (1), 1501.
- Somé, B.M., Guissou, E., Da, D.F., Richard, Q., Choisy, M., Yameogo, K.B., Hien, D.F., Yerbanga, R.S., Ouedraogo, G.A., Dabiré, K.R., et al., 2024. Mosquito ageing modulates the development, virulence and transmission potential of pathogens. *Proc. R. Soc. B* 291 (2023), 20232097.
- Styer, L.M., Carey, J.R., Wang, J.-L., Scott, T.W., 2007a. Mosquitoes do senesce: departure from the paradigm of constant mortality. *Am. J. Trop. Med. Hyg.* 76 (1), 111.
- Styer, L.M., Minnick, S.L., Sun, A.K., Scott, T.W., 2007b. Mortality and reproductive dynamics of *Aedes aegypti* (Diptera: Culicidae) fed human blood. *Vector-Borne Zoonotic Dis.* 7 (1), 86–98.
- Tsurim, I., Silberbush, A., Ovadia, O., Blaustein, L., Margalith, Y., 2013. Inter- and intra-specific density-dependent effects on life history and development strategies of larval mosquitoes. *PLoS One* 8 (3), e57875.
- Turell, M.J., 2012. Members of the *Culex pipiens* complex as vectors of viruses. *J. Am. Mosq. Control Assoc.* 28 (4s), 123–126.
- Tyndale-Biscoe, M., 1984. Age-grading methods in adult insects: a review. *Bull. Entomol. Res.* 74 (3), 341–377.
- Vaux, A. G.C., Gibson, G., Hernandez-Triana, L.M., Cheke, R.A., McCracken, F., Jeffries, C.L., Horton, D.L., Springate, S., Johnson, N., Fooks, A.R., et al., 2015. Enhanced West Nile virus surveillance in the North Kent marshes, UK. *Parasit. Vectors* 8, 1–8.
- Vinogradova, E.B., 2000. *Culex pipiens pipiens* Mosquitoes: Taxonomy, Distribution, Ecology, Physiology, Genetics, Applied Importance and Control. 2, Pensoft Publishers.
- Walter, N.M., Hacker, C.S., 1974. Variation in life table characteristics among three geographic strains of *Culex pipiens quinquefasciatus*. *J. Med. Entomol.* 11 (5), 541–550.
- Watts, D.M., Burke, D.S., Harrison, B.A., Whitmore, R.E., Nisalak, A., et al., 1987. Effect of temperature on the vector efficiency of *Aedes aegypti* for dengue 2 virus. *Am. J. Trop. Med. Hyg.* 36 (1), 143–152.
- Wilson, A.L., Courtenay, O., Kelly-Hope, L.A., Scott, T.W., Takken, W., Torr, S.J., Lindsay, S.W., 2020. The importance of vector control for the control and elimination of vector-borne diseases. *PLoS Negl. Trop. Dis.* 14 (1), e0007831.
- World Health Organization, et al., 2020. Multisectoral Approach to the Prevention and Control of Vector-Borne Diseases: A Conceptual Framework. World Health Organization <https://iris.who.int/handle/10665/331861>. License: CC BY-NC-SA 3.0 IGO.